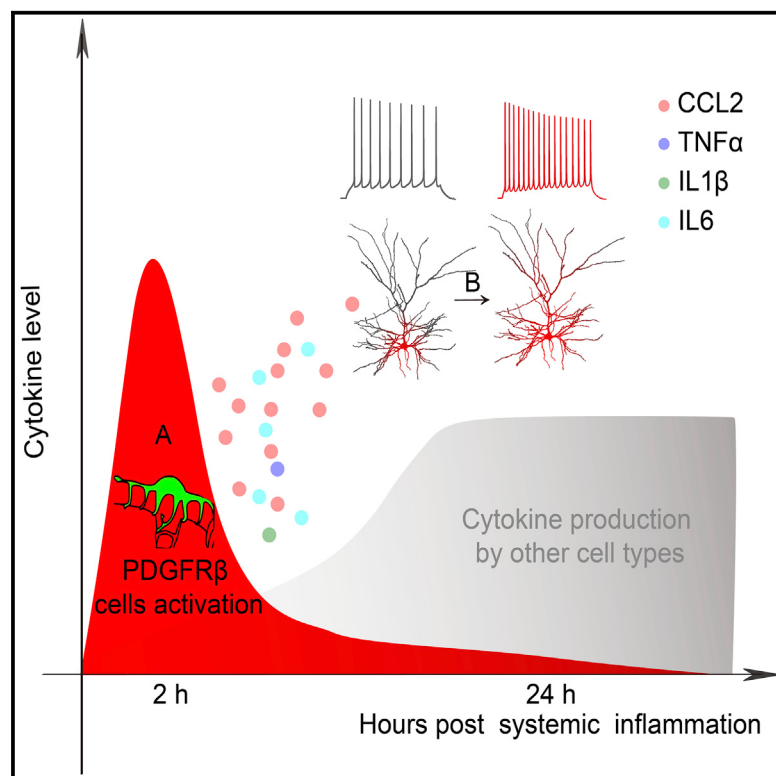


Neuron

PDGFR β Cells Rapidly Relay Inflammatory Signal from the Circulatory System to Neurons via Chemokine CCL2

Graphical Abstract



Authors

Lihui Duan, Xiao-Di Zhang,
Wan-Ying Miao, ..., Xiaoping Tong,
Wen-Hao Zhou, Xiang Yu

Correspondence

yuxiang@ion.ac.cn

In Brief

Yu and colleagues identified *Rgs5* and *Col1a1* subgroups of PDGFR β cells as early responders to neuroinflammation. These cells rapidly synthesize and release the chemokine CCL2, which in turn elevates neuronal excitability and excitatory synaptic transmission in multiple neuronal types.

Highlights

- PDGFR β cells function as initial sensors of systemic inflammation in the brain
- PDGFR β cells relay the infection signal to neurons by secreting chemokine CCL2
- *Col1a1* and *Rgs5* subgroups of PDGFR β cells are sources of *Ccl2* during early infection
- PDGFR β -specific *Ccl2* knockout blocked LPS-induced increase in synaptic transmission



PDGFR β Cells Rapidly Relay Inflammatory Signal from the Circulatory System to Neurons via Chemokine CCL2

Lihui Duan,^{1,2,6} Xiao-Di Zhang,^{1,2,6} Wan-Ying Miao,¹ Yun-Jun Sun,¹ Guoliang Xiong,^{1,2} Qiuzi Wu,¹ Guangying Li,¹ Ping Yang,⁴ Hang Yu,^{1,2} Humingzhu Li,^{1,3} Yue Wang,^{1,3} Min Zhang,¹ Li-Yuan Hu,⁴ Xiaoping Tong,⁵ Wen-Hao Zhou,⁴ and Xiang Yu^{1,2,3,7,*}

¹Institute of Neuroscience, State Key Laboratory of Neuroscience, CAS Center for Excellence in Brain Science and Intelligence Technology, Chinese Academy of Sciences, Shanghai 200031, China

²University of Chinese Academy of Sciences, Beijing 100049, China

³School of Life Science and Technology, ShanghaiTech University, Shanghai 201210, China

⁴Department of Neonatology, Children's Hospital of Fudan University, Shanghai 201102, China

⁵Department of Anatomy and Physiology, Shanghai Jiao Tong University School of Medicine, Shanghai 200025, China

⁶These authors contributed equally

⁷Lead Contact

*Correspondence: yuxiang@ion.ac.cn

<https://doi.org/10.1016/j.neuron.2018.08.030>

SUMMARY

Acute infection, if not kept in check, can lead to systemic inflammatory responses in the brain. Here, we show that within 2 hr of systemic inflammation, PDGFR β mural cells of blood vessels rapidly secrete chemokine CCL2, which in turn increases total neuronal excitability by promoting excitatory synaptic transmission in glutamatergic neurons of multiple brain regions. By single-cell RNA sequencing, we identified *Col1a1* and *Rgs5* subgroups of PDGFR β cells as the main source of CCL2. Lipopolysaccharide (LPS)- or Poly(I:C)-treated pericyte culture medium induced similar effects in a CCL2-dependent manner. Importantly, in *Pdgfrb-Cre;Ccl2^{f/f}* mice, LPS-induced increase in excitatory synaptic transmission was significantly attenuated. These results demonstrate *in vivo* that PDGFR β cells function as initial sensors of external insults by secreting CCL2, which relays the signal to the central nervous system. Through their gateway position in the brain, PDGFR β cells are ideally positioned to respond rapidly to environmental changes and to coordinate responses.

INTRODUCTION

Recent evidence demonstrating extensive crosstalk among the nervous, immune, and circulatory systems has sparked exciting research studying their interactions. Specifically, it has been shown that immune cells and molecules can cross the blood-brain barrier (BBB) under both physiological and pathological conditions (Becher et al., 2017; Klein et al., 2017; Prinz and Priller, 2017; Zhao et al., 2015). Furthermore, a number of classic immune molecules, including cytokines and cell surface molecules,

have newly identified functions in neural development and plasticity (Boulanger, 2009; Deverman and Patterson, 2009; Estes and McAllister, 2015; Shatz, 2009). Finally, cells of the nervous and immune systems have been shown to bidirectionally regulate each other (Becher et al., 2017; Dantzer et al., 2008; Klein et al., 2017; Wohleb et al., 2016).

The response to infection is a physiopathological condition under which crosstalk among the three systems is of particular relevance. Young children are especially vulnerable, with infection being a leading cause of mortality for children under 5 years of age (Liu et al., 2015). If not timely and effectively treated, systemic infection can lead to central nervous system (CNS) inflammation, resulting in encephalitis, meningitis, seizures, and sometimes coma. Long-term adverse consequences of neonatal neuroinflammation, partly attributed to excessive immune responses to systemic infection, include intellectual disability, epilepsy, autism spectrum disorder, and schizophrenia (Chandran et al., 2011; Estes and McAllister, 2015, 2016; Klein et al., 2017; Knuesel et al., 2014; Meyer et al., 2011; Vezzani et al., 2011; Xanthos and Sandkühler, 2014).

Previous studies have shown that microglia and astrocyte activation, as well as influx of monocytes into the brain parenchyma, together with the cytokines that they release, all contribute significantly to infection-induced neuroinflammation (Klein et al., 2017; Liddelow and Barres, 2017; Prinz and Priller, 2014, 2017; Salter and Stevens, 2017; Sofroniew, 2015). However, since previous studies mostly focused on the long-term effects of neuroinflammation, the early events are less well characterized. In particular, it is unknown whether a specific cell type functions as the sensor of system infection in the brain. Furthermore, it is also unknown whether specific molecule(s) released by this cell type(s) relay and/or broadcast the inflammatory signal to other cells in the brain. If such cells and signals exist, a better understanding of their mechanism and time course of action could provide a way to rapidly and effectively dampen excessive immune response during inflammation. New and effective ways to balance sufficient immune response to eliminate the external



insult, while not damaging self, are key to more effective treatment and better prognosis.

Here we showed that the cell type first activated in the CNS in response to systemic inflammation is the PDGFR β cell, the mural cell of blood vessels. By single-cell RNA sequencing (RNA-seq), we showed that *Col1a1* and *Rgs5* subgroups of PDGFR β cells are the main source of CCL2. Within 2 hr of inducing systemic inflammation, PDGFR β cells secreted CC chemokine ligand 2 (CCL2, also known as monocyte chemotactic protein-1, MCP1), which in turn increased total neuronal excitability by promoting excitatory synaptic transmission in glutamatergic neurons of multiple brain regions. Importantly, when *Ccl2* was conditionally knocked out from PDGFR β cells, the effect of LPS-induced increase in excitatory synaptic transmission was significantly attenuated. Together, these results provide *in vivo* demonstration that *Col1a1* and *Rgs5* subgroups of PDGFR β cells function as initial sensors to external insults by secreting CCL2, which subsequently relays the inflammatory signal to the CNS.

RESULTS

Astrocytes and Microglia Are Not the Main Sources of CCL2 during Early Neuroinflammation

To examine the early effects of systemic inflammation, we intraperitoneally (i.p.) injected postnatal day 14 (P14) mice with varying doses of agents commonly used to mimic infection by bacteria and/or viruses, including lipopolysaccharides (LPS), double-stranded RNA (dsRNA; Poly(I:C)), or CpG DNA (ODN 1668), to stimulate Toll-like receptor TLR4, TLR3, or TLR9 pathways (Kawai and Akira, 2010), respectively. Hippocampal mRNA levels of proinflammatory cytokines and chemokines previously reported to mediate responses to inflammation in the brain (Breder et al., 1994; Erickson and Banks, 2011; Nadeau and Rivest, 1999; Quan et al., 1998b; Thibeault et al., 2001; Vallières and Rivest, 1997), including *Ccl2*, tumor necrosis factor α (*Tnf α*), interleukin 1 β (*Il1 β*), and *Il6*, were significantly elevated 2 hr following injections (Figure S1). Since the effect of all cytokines maxed out at 10 mg/kg, we used this dose to examine the time course of responses. All agents elevated mRNA and protein expression of the cytokines, with variability in the extent of change and in the time course (Figure S2). Of the cytokines examined, *Ccl2* mRNA and CCL2 protein showed the highest fold change in response to stimulation by all three agents (Figure S2). In absolute quantitation, 2 hr following stimulation by each of three agents, *Ccl2* mRNA copy number and CCL2 protein concentration were both the highest (Figures 1A and 1B). The consistent increase in CCL2 level across multiple systemic inflammation models suggest that it may be a key signaling molecule in the brain during the inflammatory process. Since we are most interested in early responses, for the remainder of this study, we focused on the 2 hr time point and used 10 mg/kg of LPS or Poly(I:C).

We confirmed, using *in situ* hybridization, that the *Ccl2* mRNA level was significantly elevated in the brain of P14 mice 2 hr after LPS injection (Figures S3A–S3C). Using a knockin mouse line expressing RFP under the endogenous *Ccl2* promoter (*Ccl2-RFP flox*), we further showed that CCL2 protein (CCL2-2A-RFP)

was also highly expressed 2 hr following LPS injection and colocalized with *Ccl2* mRNA (Figures 1C, S3D, and S3E; 45.56% \pm 4.50% colocalization with respect to [w.r.t.] total mRNA, 44.49% \pm 7.74% w.r.t. total RFP).

The *in situ* results also provided spatial information for identifying the cell type that expressed *Ccl2*. Since astrocyte and microglia activation during neuroinflammation is well documented (Liddelow and Barres, 2017; Prinz and Priller, 2014; Salter and Stevens, 2017; Sofroniew, 2015), we first examined colocalization between *Ccl2* mRNA and the microglia marker ionized calcium binding adaptor molecule 1 (Iba1) or the astrocyte marker glial fibrillary acidic protein (GFAP) 2 hr following either LPS or Poly(I:C) injection. To our surprise, colocalization, defined as overlap between the two signals at the pixel level, was low for either marker (LPS: GFAP, 11.03% \pm 0.84%, Iba1, 15.27% \pm 6.26%; Poly(I:C): GFAP, 9.86% \pm 1.36%, Iba1, 21.76% \pm 2.12%; Figures 1D–1Q). To aid visualization, we also plotted fluorescence intensity of *Ccl2* mRNA and Iba1/GFAP immunostaining along indicated lines. The plots clearly showed that while *Ccl2* and Iba1/GFAP signals are often juxtaposed, they mostly did not colocalize. Consistently, we only observed significant increase in GFAP or Iba1 immunostaining 24 hr following LPS injection and no obvious astrogliosis or microgliopathy at the earlier 2 hr or 6 hr time points (Figure S4). Thus, astrocytes and microglia are unlikely to be the main source of CCL2 during early neuroinflammation.

PDGFR β Cells, Not Endothelial Cells, Express CCL2 during the Initial Phase of Neuroinflammation

Our *in situ* hybridization results showed a high *Ccl2* level surrounding the meninges (Figure S3A) and blood vessels (Figure S3B). A previous study reported elevated *Ccl2* following LPS injection in regions including these. Based on colocalization between radioactively labeled *Ccl2* *in situ* probe and immunostaining for an endothelial cell marker, endothelial cells were thought to be the source of CCL2 (Thibeault et al., 2001). However, we observed relatively little colocalization between *Ccl2* and the endothelial cell marker Glut1, even though sometimes *Ccl2*- and Glut1-positive cells were juxtaposed (LPS: 12.82% \pm 1.36%; Poly(I:C): 7.75% \pm 3.17%; Figures 2A–2C, 2G–2I, 2M, and 2N). Much higher colocalization—close to 50%—was observed between *Ccl2* and platelet-derived growth factor receptor β (PDGFR β) (LPS: 46.91% \pm 3.76%; Poly(I:C): 49.51% \pm 2.87%; Figures 2D–2F and 2J–2N). PDGFR β cells, the mural cells of blood vessels, are located along intervals within the vascular basement membrane. Given the physical proximity between mural cells and endothelial cells and the resolution limit of autoradiography (Thibeault et al., 2001), our data are not inconsistent with previous reports.

To confirm *Ccl2* expression in PDGFR β cells, we performed *in situ* hybridization using *Pdgfrb-Cre;Ai9* mice (Cuttler et al., 2011), previously shown to label mural cells in the brain (Hartmann et al., 2015; Jung et al., 2018). *Ccl2* mRNA colocalized with *Pdgfrb-Cre;Ai9* at the meninges and around blood vessels (Figure 2O). High-level colocalization was also found between CCL2-2A-RFP and PDGFR β antibody (Figure 2P; 52.38% \pm 8.45% w.r.t. RFP). PDGFR β antibody staining also highly colocalized with RFP in *Pdgfrb-Cre;Ai9* mice (Figure S3F; 69.42% \pm 6.67%

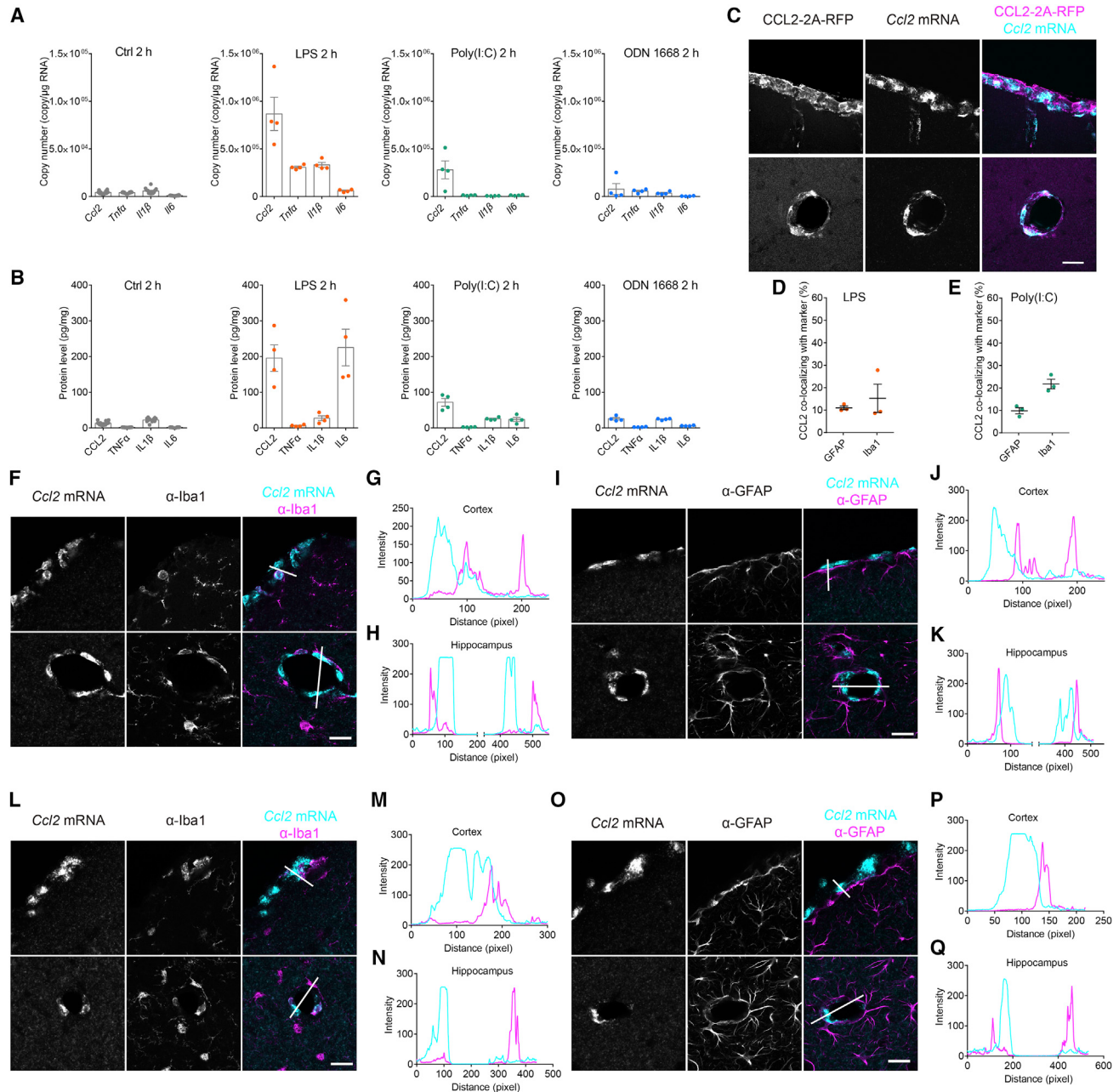


Figure 1. CCL2 Is Highly Expressed during Early Systemic Inflammation, but Mostly Does Not Localize to Microglia or Astrocytes

(A and B) Absolute mRNA copy number (A) and protein level (B) of cytokines in the hippocampus of P14 mice 2 h after i.p. injection of 10 mg/kg LPS, Poly(I:C), ODN 1668, or saline (Ctrl) (each data point represents one mouse, 4–12 mice per group).

(C) Representative images of Cc2 mRNA co-labeling with CCL2-2A-RFP in Cc2-RFP^{flox} mice 2 h after LPS injection. In this and subsequent images, top rows are from the meninges surrounding the cerebral cortex; bottom rows are from blood vessels in the hippocampus.

(D and E) Percentage of colocalization between Cc2 mRNA and GFAP or Iba1 after LPS (D) or Poly(I:C) (E) injection (3 mice per group).

(F, I, L, and O) Representative images of Cc2 mRNA co-labeling with Iba1 or GFAP 2 h after LPS (F and I) or Poly(I:C) (L and O) injection.

(G, H, J, K, M, N, P, and Q) Plots of pixel intensity along the white line from top (G, J, M, and P) and bottom (H, K, N, and Q) rows of images to the left of each plot, colors as in merged images.

Scale bars, 20 μm.

In this and all subsequent figures, data are presented as mean ± SEM; *p < 0.05, **p < 0.01, ***p < 0.001.

See also Figures S1–S4.

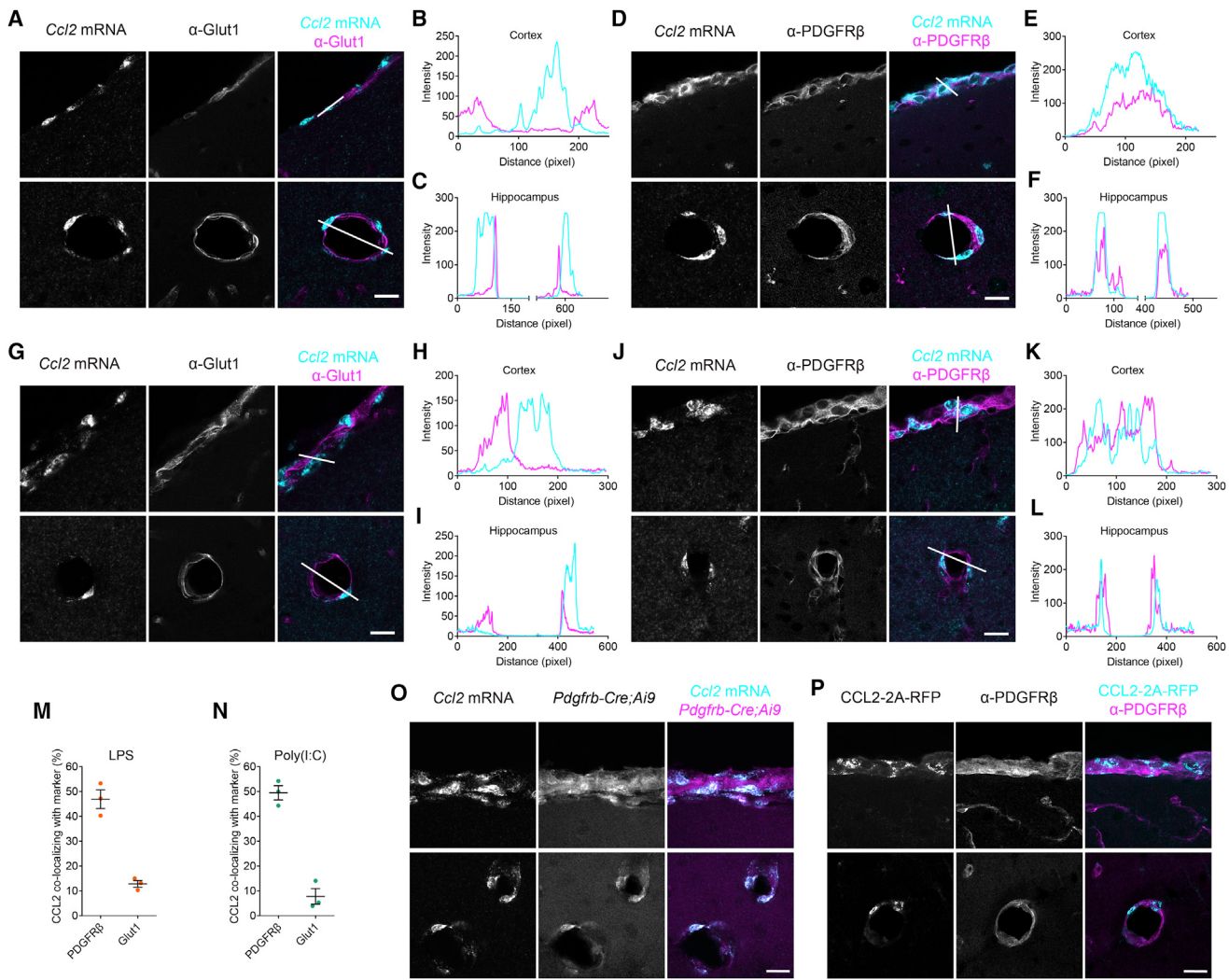


Figure 2. In Response to Acute Systemic Inflammation, PDGFR β Cells, Not Endothelial Cells, Secrete CCL2

(A, D, G, and J) Representative images of *Ccl2* mRNA co-labeling with Glut1 (A and G) or PDGFR β (D and J) 2 hr after LPS (A and D) or Poly(I:C) (G and J) injection. (B, C, E, F, H, I, K, and L) Plots of pixel intensity along the white line from top (B, E, H, and K) and bottom (C, F, I, and L) rows of images to the left of each plot.

(M and N) Percentage of colocalization between *Ccl2* mRNA and PDGFR β or Glut1 after LPS (M) or Poly(I:C) (N) injection (3 mice per group).

(O and P) Representative images of *Ccl2* mRNA in *Pdgfb-Cre;Ai9* mice (O) or CCL2-2A-RFP colocalizing with PDGFR β after LPS injection (P).

Scale bars, 20 μ m.

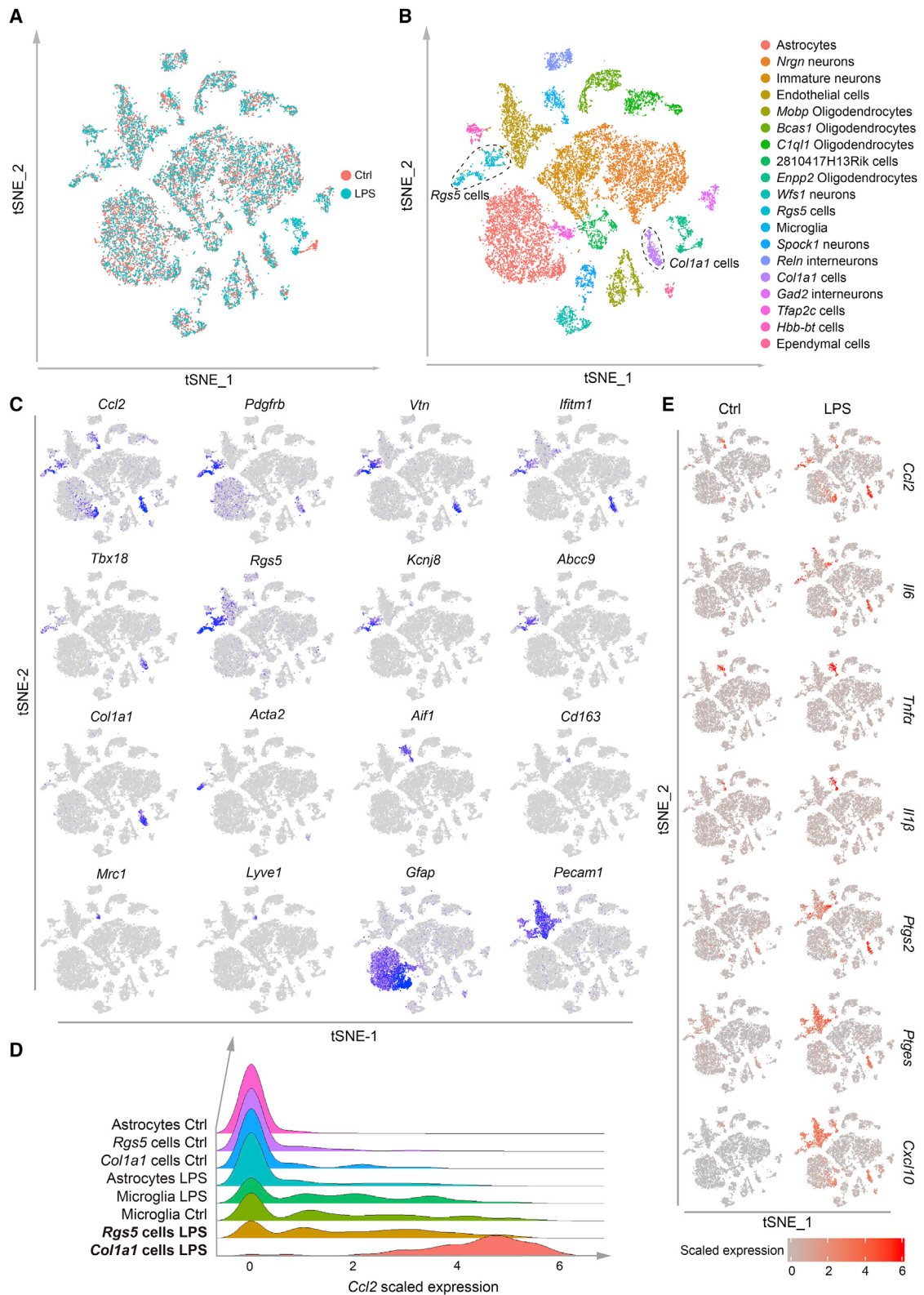
See also Figure S3.

w.r.t. *Pdgfb-Cre;Ai9* and $74.60\% \pm 1.03\%$ w.r.t. PDGFR β antibody), consistent with previous reports (Cuttler et al., 2011; Hartmann et al., 2015) and further confirming specificity of *Pdgfb-Cre* in labeling mural cells.

Rgs5 and Col1a1 Subtypes of PDGFR β Cells Express *Ccl2*

Mural cells mostly comprise pericytes and vascular smooth muscle cells (Armulik et al., 2011; Hartmann et al., 2015; Jung et al., 2018). Pericytes align blood microvessels, are located along intervals within the vascular basement membrane, and have been shown to be critical for maintaining the BBB's integrity (Armulik et al., 2010, 2011; Bell et al., 2010; Daneman et al., 2010;

Rustenhoven et al., 2017; Sweeney et al., 2016). Vascular smooth muscle cells form relatively continuous cell layers around arteries and veins and regulate blood vascular tone and vessel diameter, blood pressure, and flow (Gaengel et al., 2009). Do both cell types secrete *Ccl2*? Are there other perivascular cells that also secrete *Ccl2*? To further characterize these cells, we dissociated the hippocampi of P14 mice 2 hr following LPS or saline (Ctrl) injection and performed single-cell RNA-seq, using previously described methods (Zeisel et al., 2015). Single cells were captured on the 10X Chromium instrument. From three independent experiments, we obtained 9,957 cells for the Ctrl group and 9,675 cells for the LPS group after quality control. The batch effect was regressed out using Seurat (Satija



(legend on next page)

et al., 2015). LPS and Ctrl groups were aligned and combined using Seurat (Butler et al., 2018) (Figure 3A). Unsupervised clustering and t-distributed stochastic neighbor embedding (tSNE) plot were used to characterize and visualize transcriptional heterogeneity among all cells (see STAR Methods for details). Nineteen clusters were identified (Figure 3B) and named according to commonly used cell-type names or, where unclear, the most significant marker gene of the cluster. Cells were assigned to clusters based on sharing a group of specifically expressed genes.

Consistent with *in situ* results, *Ccl2* expression was highly similar to that of reported pericyte markers, including *Pdgfrb*, *Vtn*, *Ifitm1*, *Foxc1*, *Tbx18*, *Rgs5*, *Kcnj8*, *Abcc9*, and *Col1a1* (Figure 3C) (Armulik et al., 2011; Vanlandewijck et al., 2018). *Ccl2* cells did not express the smooth muscle cell marker *Acta2* (Figure 3C). Myeloid cells (microglia or perivascular macrophages) (Ajami et al., 2018; Mrdjen et al., 2018) are key players of neuro-inflammation in the CNS. However, *Ccl2* was not significantly induced in cells expressing microglia markers (*Iba1/Aif1*) or perivascular macrophages markers (*Cd163*, *Cd206/Mrc1*) (Figures 3C and 3D). Expression of *Ccl2* in both Ctrl and LPS groups could be due to dissection-induced damage (Saijo and Glass, 2011), as we did not observe high-level colocalization between *Ccl2* and *Iba1* (Figure 1). *Ccl2* expression was not detected in lymphatic vessel endothelial cells (*Lyve1*) or endothelial cells (*Pecam1*) (Figure 3C).

Analysis of *Ccl2* expression according to the 19 identified cell clusters showed high expression in *Col1a1* cells, microglia, *Rgs5* cells, and astrocytes (Figure S5A). *Ccl2* expression was similarly high in microglia in Ctrl and LPS samples (Figures 3D and 3E), while its LPS-induced expression in astrocytes was much lower than that of *Rgs5* and *Col1a1* cells (Figure 3D). *Ccl2* was the most significantly induced gene in *Col1a1* cells and ranked within the top ten genes in *Rgs5* cells (Table S1). What are *Col1a1* and *Rgs5* cells? The top ten marker genes in *Col1a1* cells (Ctrl 176 cells; LPS 219 cells) are *Col1a1*, *Col1a2*, *Dcn*, *Col3a1*, *Cp*, *Ifitm1*, *Nupr1*, *Cyp1b1*, *Lum*, and *Pcolce* (Table S1). *Col1a1* cells were previously identified as a subtype of *Pdgfrb* cells by single-cell RNA-seq (Bifari et al., 2017). A recent report identified *Col1a1* as a marker of perivascular fibroblast-like cells (Vanlandewijck et al., 2018). These cells are in close association with arteries, arterioles, veins, and venules; are non-overlapping with endothelial cells and mural cells; and are located between the vessel wall and astrocytes endfeet (Vanlandewijck et al., 2018). In addition to *Col1a1*, this cluster also shares the markers *Col1a2*, *Dcn*, *Col3a1*, and *Lum* with perivascular fibroblast-like cells (Vanlandewijck et al., 2018). *Col1a1* cells also express identified pericyte markers, including *Pdgfrb*, *Vtn*, *Ifitm1*, and *Tbx18* (Figure 3C).

Rgs5 cells (Ctrl 265 cells; LPS 316 cells) are characterized by expression of *Rgs5*, *Vtn*, *Myl9*, *Higd1*, *Ndufa4l2*, *Kcnj8*, *Sod3*,

Ebf1, *Apold1*, and *Cox4i2*. The top 50 markers (Table S1) include a number of identified pericyte markers, including *Rgs5*, *Vtn*, *Kcnj8*, *Pdgfrb*, *Abcc9*, and *Tbx18* (Figure 3C). Thus, the *Rgs5* cell cluster includes a significant proportion of cells classically identified as pericytes. We say “include” because a fraction of these cells (35.5% of Ctrl and 27.2% of LPS group) also express the vascular smooth muscle marker *Acta2* (Figure 3C).

Together, our results identified *Col1a1* cells as perivascular fibroblast-like cells and *Rgs5* cells as a pericyte-including cell type. Since *Vtn* is expressed by both *Rgs5* and *Col1a1* cells and is a recently reported marker of *Pdgfrb* and NG2 double positive cells (He et al., 2016), we examined colocalization of *Vtn* mRNA with CCL2-2A-RFP (Figure 4A) and with *Pdgfrb-Cre;Ai9* (Figures 4B and S5D). The results showed high-level colocalization of *Vtn* with both markers.

In situ hybridization of *Col1a1* and *Ccl2*, together with immunohistochemistry for PDGFR β , showed that *Col1a1* colocalized well with both (Figure 4C). Consistent with previous characterization of perivascular fibroblast-like cells (Vanlandewijck et al., 2018), *Col1a1* cells are mainly located at meninges and large vessels. *Ccl2*-expressing and *Col1a1*-negative PDGFR β cells, most likely representing *Rgs5*-positive pericytes, are mainly located at small vessels (Figure 4C).

To further analyze *Pdgfrb*-expressing cells (defined as cells with equal/higher expression of *Pdgfrb* than the mean *Pdgfrb* expression in all cells), we performed unsupervised clustering of these cells by Seurat (Figure S6A). *Col1a1* and *Rgs5* cells remain the main sources of *Ccl2* after LPS treatment. *Rgs5* cells were further divided into *Rgs5(A)* and *Rgs5(B)* cells. *Rgs5(A)* cells have high expression of pericyte markers *Abcc9* and *Kcnj8*, while *Rgs5(B)* cells expressed the smooth muscle cell marker *Acta2* (Figure S6B). A significant number of astrocytes also expressed *Pdgfrb* above the cutoff threshold for this analysis (Figure S6A), though their *Pdgfrb* expression was lower than that of other cell types (Figure S6B). *Pdgfrb* expression in astrocytes has been reported in previous single-cell RNA-seq studies (Zeisel et al., 2015; Zhang et al., 2014). However, PDGFR β immunostaining or *Ai9* expression in *Pdgfrb-Cre;Ai9* mice was not observed in cells with classical astrocyte morphology in our samples and not previously reported. *Ccl2* expression in *Pdgfrb*-expressing astrocytes was not significantly induced by LPS (Figure S6B).

In addition to *Ccl2*, a number of other cytokines and enzymes have previously been shown to be induced along blood vessels during acute infection, including *Tnf α* (Breder et al., 1994; Nadeau and Rivest, 1999), *Il6* (Vallières and Rivest, 1997), *Il1 β* (Ericsson et al., 1995; Nakamori et al., 1994; Quan et al., 1998b), *Pegs2* (Cao et al., 1995; Quan et al., 1998a), *Ptges* (Ek et al., 2001), and *Cxcl10* (Blank et al., 2016). In our dataset,

Figure 3. Identification of *Rgs5* Cells and *Col1a1* Cells as the Main Cell Types in the Brain that Respond to LPS during the Acute Phase of Infection, Using Single-Cell RNA-Seq

- (A) tSNE plots of 19,632 mouse hippocampal cells, split between 2 hr Ctrl (9957 cells) and 2 hr LPS *in vivo* stimulated (9675 cells) conditions.
- (B) Visualization of 19 major classes of cells using tSNE. Each point represents a single cell (droplet barcode) colored by cluster assignment. *Rgs5* cells: 581 cells. *Col1a1* cells: 395 cells.
- (C and E) Expression of different genes projected onto tSNE plots. All cells are included in (C). Color scaled for each gene with log normalized expression level (E).
- (D) Ridge plot of *Ccl2* expression in high-expressing cell clusters.
- See also Figures S5 and S6 and Table S1.

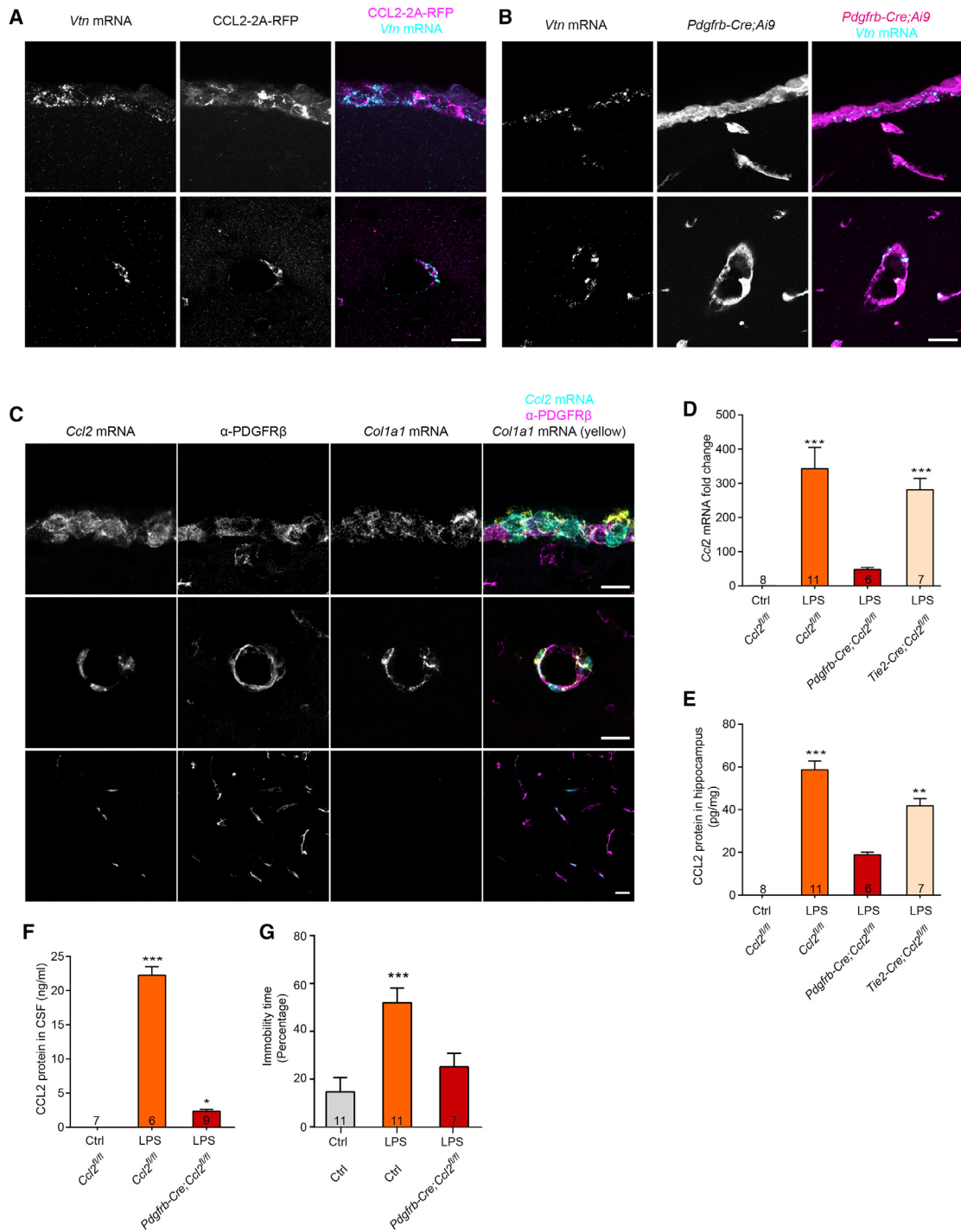


Figure 4. Identification of PDGFR β Cells as the Main Cell Types in the Brain that Respond to LPS during the Acute Phase of Infection

(A and B) Representative images of *Vtn* mRNA co-labeling with CCL2-2A-RFP (A) or *Pdgfrb-Cre; Ai9* (B) 2 hr after LPS. Top rows are from the meninges surrounding the cerebral cortex; bottom rows are from blood vessels in the hippocampus.

(C) Representative images of *Ccl2* mRNA co-labeling with *Col1a1* mRNA and PDGFR β . Third row is from small blood vessels in the cerebral cortex.

(D and E) Fold change in *Ccl2* mRNA (D) and CCL2 protein (E) in the hippocampus of *Pdgfrb-Cre; Ccl2^{fl/fl}* or *Tie2-Cre; Ccl2^{fl/fl}* mice 2 hr following LPS injection (6–11 mice per group, n as indicated; Kruskal-Wallis test, Dunn's post hoc test).

(F) CCL2 level in the CSF of *Pdgfrb-Cre; Ccl2^{fl/fl}* adult mice 2 hr following LPS injection (6–9 mice per group, n as indicated; Kruskal-Wallis test, Dunn's post hoc test).

(legend continued on next page)

Tnfα was mainly expressed in microglia but at similar levels in Ctrl and LPS groups (Figure 3E). *Il6* was also mostly expressed in PDGFR β cells but at a lower level than *Ccl2*. *Cxcl10*, *Ptgs2*, *Cox2*, and *Ptges* were expressed in *Col1a1* cells, *Rgs5* cells, and endothelial cells.

PDGFR β Cells Are the Main Source of CCL2 during Early Neuroinflammation

The single-cell RNA-seq results showed that the *Col1a1* and *Rgs5* subclasses of PDGFR β cells are the main sources of CCL2 during early inflammation. To assay this requirement functionally, we conditionally knocked out *Ccl2* from PDGFR β cells in *Pdgfrb-Cre;Ccl2^{f/f}* mice. LPS-induced increase in hippocampal *Ccl2* mRNA and CCL2 protein expression was significantly attenuated at 2 hr (Figures 4D and 4E), suggesting that PDGFR β cells are the main source of CCL2 during early neuroinflammation. In contrast, when *Ccl2* was conditionally knocked out from endothelial cells in *Tie2-Cre;Ccl2^{f/f}* mice, hippocampal *Ccl2* was not significantly affected (Figures 4D and 4E). These results provide important *in vivo* evidence that PDGFR β cells, but not endothelial cells, are the main source of CCL2 during early neuroinflammation. LPS-induced CCL2 was also detected in the cerebral spinal fluid (CSF) at 2 hr (Figure 4F). High CSF CCL2 during early systemic inflammation allows it to rapidly reach many regions in the brain and mediate downstream effects. Importantly, conditional knockout of *Ccl2* from PDGFR β cells significantly attenuated this effect (Figure 4F), demonstrating a critical contribution of these cells to CSF CCL2 level.

A salient response to infection is sickness behavior (Dantzer et al., 2008; Wohleb et al., 2016), comprising lethargy, social withdrawal, and other changes that decrease energy expenditure, with the likely function of promoting survival and/or not passing the infection to other individuals in the group. Previous reports showed that LPS-injected mice were less mobile in the tail-suspension test (Dantzer et al., 2008). Here we showed that 2 hr after LPS injection, LPS-induced reduction in mobility was significantly attenuated in *Pdgfrb-Cre;Ccl2^{f/f}* mice to a level similar to control, non-LPS-injected mice (Figure 4G). These results suggest that CCL2 secretion by PDGFR β cells during the early phase of inflammation may have important physiological functions.

CCL2 Rapidly Increases Excitatory Synaptic Transmission

Having identified PDGFR β cells as initial responders during early neuroinflammation and CCL2 as their main signaling molecule, we next asked what cells CCL2 target. We recorded AMPA-type glutamate-receptor-mediated miniature excitatory postsynaptic currents (mEPSCs) from hippocampal CA1 pyramidal neurons in acute brain slices of P14 mice 2 hr after i.p. injection of LPS or Poly(I:C). The frequency of mEPSC was significantly increased, while its amplitude was not significantly affected (Figures 5A, 5B, S7A, and S7B). Perfusion of CCL2 (100 ng/mL) (Gao

et al., 2009; Gosselin et al., 2005) onto CA1 pyramidal neurons had similar effects, significantly increasing mEPSC frequency over the course of minutes (Figures 5E and 5F). Simplistically, mEPSC amplitude correlates with the density/conductance of postsynaptic receptors at individual synapses, while mEPSC frequency reflects the number of functional synapses and/or release probability of individual synapses. Both changes can have pre- and postsynaptic origins. For instance, an increase in mEPSC frequency could be due to unsilencing of “silent” synapses that contain NMDA receptors but lack AMPA receptors (Malenka and Nicoll, 1997). Both mEPSC frequency and amplitude contribute to the total synaptic strength of the neuron, which can be measured as total charge transfer per second. CCL2 application significantly increased total synaptic charge (Figure 5I).

To further examine whether CCL2 application increased the total synaptic strength of synchronized release, we measured evoked EPSC following minimal stimulation of nearby stratum radiatum. CCL2 application significantly increased the amplitude of the evoked AMPA EPSC (Figures 5J and 5K). CCL2 application also increased the AMPA/NMDA ratio, a measure of the size of the evoked AMPA current, as a ratio of the NMDA current, suggesting a primarily postsynaptic effect through unsilencing of “silent” synapses (Figures 5L and 5M). Paired-pulse ratio (PPR), a measure of presynaptic release probability, was not affected (Figures 5N and 5O). Inhibitory synaptic transmission, measured as the frequency and amplitude of miniature inhibitory postsynaptic currents (mIPSC), also was not significantly affected (Figures S7C and S7D).

Do these synaptic changes affect neuronal firing? Because spontaneous firing is very low in CA1 pyramidal neurons, we measured neuronal firing in response to step depolarizing current injections. Both LPS injection and CCL2 perfusion onto hippocampal slices increased total neuronal excitability (Figures 5C, 5D, 5G, and 5H), which has contributions from excitatory and inhibitory synaptic inputs, as well as the neuron’s intrinsic electrical properties. Consistent with the observed increase in excitatory synaptic transmission and lack of change in inhibitory synaptic transmission (Figures 5E, 5F, S7C, and S7D), the effects of CCL2 were blocked by the AMPA receptor inhibitor NBQX, but not the GABA_A receptor inhibitor gabazine (Figures S7E–S7H). CCL2 did not significantly affect intrinsic excitability (Figures S7I and S7J).

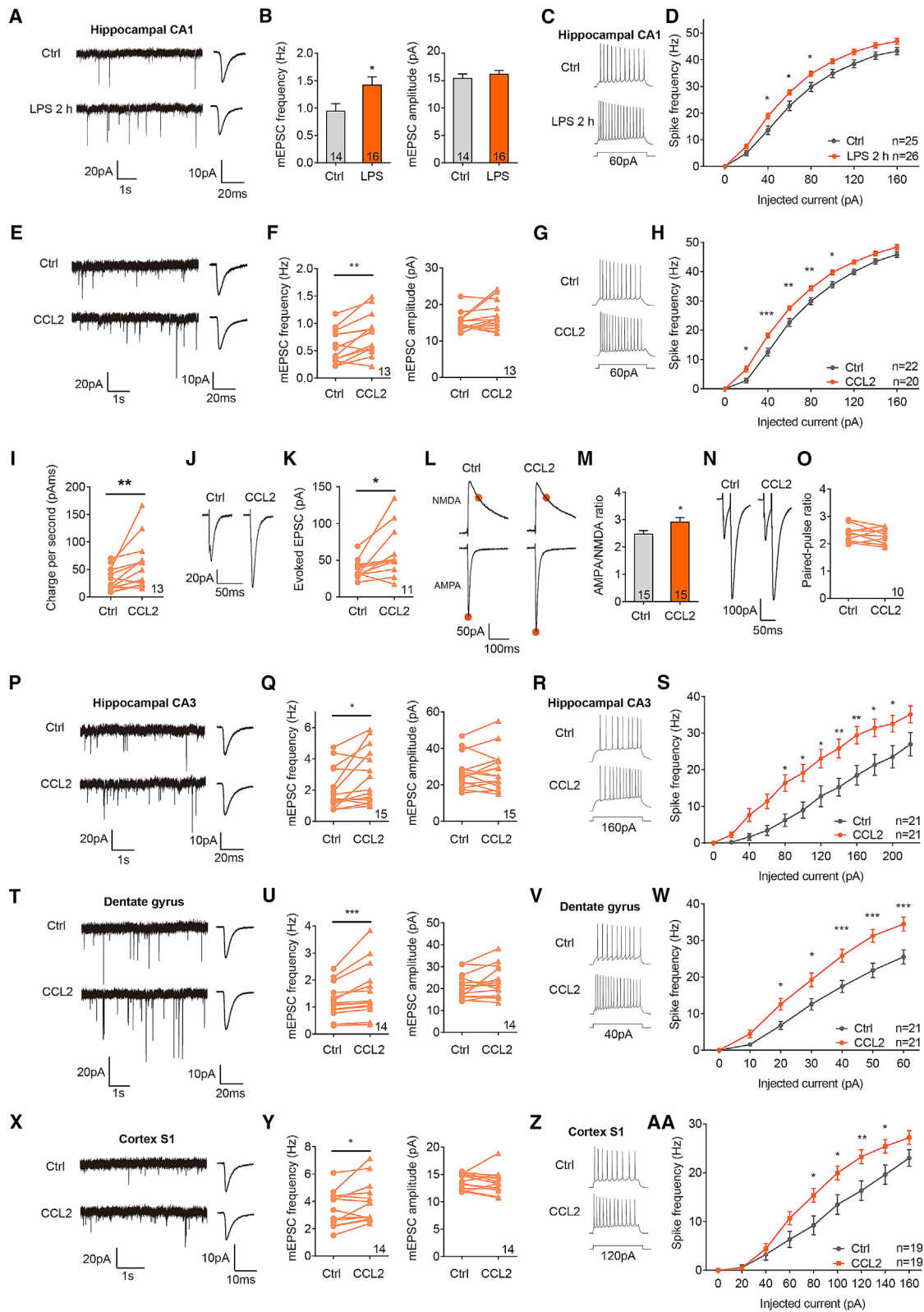
Together, the above results demonstrate that CCL2 primarily affects CA1 pyramidal neurons by upregulating their excitatory synaptic transmission. CCL2 application onto hippocampal CA3 pyramidal neurons, dentate gyrus granule cells, or layer 2/3 pyramidal neurons of the primary somatosensory cortex (Figures 5P–5AA) all enhanced excitatory synaptic transmission and total neuronal excitability, suggesting a global effect of this molecule in regulating excitatory synaptic transmission in the brain.

The effect of CCL2 is mediated through CC chemokine receptor 2 (CCR2), its predominant receptor (Réaux-Le Goazigo et al.,

(G) Percentage of immobility time in tail-suspension test of *Pdgfrb-Cre;Ccl2^{f/f}* and control mice; conditions as indicated (7–11 mice per group, n as indicated; Kruskal-Wallis test, Dunn’s post hoc test).

Scale bars, 20 μ m.

See also Figures S5 and S6.



(legend on next page)

2013; Zlotnik and Yoshiie, 2012), as CCL2 application onto brain slices from *Ccr2* knockout mice did not affect mEPSC frequency or total neuronal excitability (Figures 6A–6D). CCR2 expression has been described in neurons of the cerebral cortex and hippocampus (Réaux-Le Goazigo et al., 2013). When the level of CCR2 was specifically reduced in hippocampal pyramidal neurons using RNA interference (*Ccr2* RNAi⁺; Figure S7K for verification), CCL2-induced increase in mEPSC frequency was blocked (Figures 6E and 6F), while that of neighboring uninfected neurons (*Ccr2* RNAi⁻) was not affected (Figures 6G and 6H). Thus, postsynaptic and cell-autonomous expression of CCR2 is required for mediating the effect of CCL2. CCR2 is a G-protein-coupled receptor that, once activated, can lead to intracellular calcium release through phospholipase C (PLC) and inositol triphosphate signaling (Kuang et al., 1996). Bath application of the PLC inhibitor U73122 (10 μM) or intracellular loading of the calcium chelator BAPTA (5 mM) into the postsynaptic cell both completely blocked the effect of CCL2 application on increasing mEPSC frequency (Figures 6I–6L). In addition to demonstrating the importance of calcium in mediating the effects of CCL2, this result provides further evidence that CCL2 mostly mediates its effects through postsynaptic mechanisms.

Pericyte-Secreted CCL2 Regulates Excitatory Synaptic Transmission and Total Neuronal Excitability

Could CCL2 secreted by PDGFRβ cells regulate excitatory synaptic transmission? PDGFRβ cells are mostly composed of pericytes and smooth muscle cells. When we stimulated primary cultures of human brain vascular pericytes (HBVPs) with 10 μg/mL LPS or Poly(I:C) for 1 to 4 hr, expression of *CCL2*, *IL1β*, and *IL6* was significantly increased, with fold changes in *CCL2* being the greatest (Figures S8A–S8C). *TNFα* was undetectable under basal conditions in these cells. Poly(I:C) stimulation of HBVP led to greater fold changes in the cytokines as compared to LPS (Figures S8A–S8C, compare with Figures S2A and S2B), possibly due to increased expression of Poly(I:C) receptor *TLR3* (Figures S8D and S8E), activating positive feedback loops.

Consistently, CCL2 protein level was also significantly elevated, as measured by immunocytochemistry (Figures S9A–S9D). Importantly, nuclear transfer of NFκB, a signature response of LPS and Poly(I:C), can be detected as early as 0.5 hr following either treatment (Figures S9E–S9H), demonstrating the rapid responsiveness of pericytes. In contrast, stimulation of human brain vascular smooth muscle cells (HBVSMCs) with LPS elevated *CCL2* levels much less effectively, consistent with the single-cell RNA-seq results (Figure S6B), although *IL1β* and *IL6* expression increased significantly (Figures S8F–S8H).

To measure the effect of pericyte-secreted medium on synaptic transmission, we treated HBVP with LPS or Poly(I:C) for 2 hr, washed out the agents (to avoid confounding effects of the agents themselves), and incubated the treated HBVP with extracellular solution (ECS) for 4 hr. The pericyte-infused ECS, which contained a significant amount of CCL2 (Figure 7A), effectively increased mEPSC frequency and total neuronal excitability (Figures 7B–7E). Importantly, when ECS was pre-incubated with CCL2 antibody to sequester CCL2 (Figure 7F), these effects were completely abolished (Figures 7G–7J). As control, CCL2 antibody application alone had no significant effects (Figures 7K and 7L). These results, together with the inability of HBVSMC to secrete CCL2, demonstrate a critical role of pericyte-secreted CCL2 in regulating excitatory synaptic transmission.

Ccl2 Knockout in PDGFRβ Cells *In Vivo* Blocks LPS-Induced Increase in Synaptic Transmission

Having shown that pericyte-secreted CCL2 was necessary and sufficient for inducing changes in excitatory synaptic transmission, we next asked whether this was also the case *in vivo*. Under control conditions, *Ccl2* knockout (*Ccl2*^{-/-}) mice and *Pdgfrb-Cre;Ccl2*^{f/f} mice have similar levels of synaptic transmission as compared with control mice (Figures S7L–S7O). Following LPS injection, however, *Ccl2*^{-/-} mice exhibited significantly lower mEPSC frequency and reduced total neuronal excitability (Figures 8A–8D), as compared with littermates. Similarly, *Pdgfrb-Cre;Ccl2*^{f/f} mice injected with LPS exhibited lower mEPSC

Figure 5. Inflammation-Induced CCL2 Promotes Excitatory Synaptic Transmission and Neuronal Excitability in CA1 Pyramidal Neurons

(A and B) Representative traces and averaged waveforms (A) and summary graphs (B) of mEPSC recordings from saline (Ctrl) or LPS-injected mice (14–16 cells from 3 mice per group; Mann-Whitney test).

(C and D) Representative traces (C) and summary graphs (D) of firing responses to stepwise current injections of Ctrl or LPS-injected mice (25–26 cells from 3 mice per group; two-way ANOVA, Bonferroni post hoc test).

(E and F) Representative traces (E) and summary data (F) of the effect of CCL2 on mEPSC frequency and amplitude. Ctrl recordings are from 0 to 5 min before CCL2 application; CCL2 recordings are from 5 to 10 min after CCL2 application (13 cells from 3 mice; Wilcoxon matched-pairs signed rank test).

(G and H) Representative traces (G) and summary data (H) of firing responses to stepwise current injections with or without bath application of CCL2 (20–22 cells from 3 mice; two-way ANOVA, Bonferroni post hoc test).

(I) Synaptic total charge transferred per second, calculated from data in (F) (Wilcoxon matched-pairs signed rank test).

(J and K) Representative traces (J) and summary data (K) of evoked EPSCs from the hippocampal Schaffer collateral-CA1 synapses under minimal stimulation before and after CCL2 application (11 cells from 5 mice; Wilcoxon matched-pairs signed rank test).

(L and M) Representative traces (L) and summary data (M) of evoked AMPA-EPSC (holding at −70 mV) and NMDA-EPSC (holding at +40 mV) from hippocampal Schaffer collateral-CA1 synapses, recorded in aCSF with or without CCL2. Filled circles indicate time points at which measurements were taken (15 cells from 4 mice per group; Student's t test).

(N and O) Representative traces (N) and summary data (O) of paired-pulse ratio recordings in the hippocampal Schaffer collateral-CA1 synapse at 25 ms intervals prior to (Ctrl) and during CCL2 application (10 cells from 3 mice; Wilcoxon matched-pairs signed rank test).

(P, Q, T, U, X, and Y) Representative traces (P, T, X) and summary data (Q, U, Y) of mEPSC recordings from brain regions as indicated, before and after CCL2 application (14–15 cells from 3–4 mice per condition; Wilcoxon matched-pairs signed rank test).

(R, S, V, W, Z, and AA) Representative traces (R, V, Z) and summary data (S, W, AA) of firing responses to stepwise current injections, with or without CCL2 application. Brain regions as indicated (19–21 cells from 3–4 mice per condition; two-way ANOVA, Bonferroni post hoc test).

See also Figure S7.

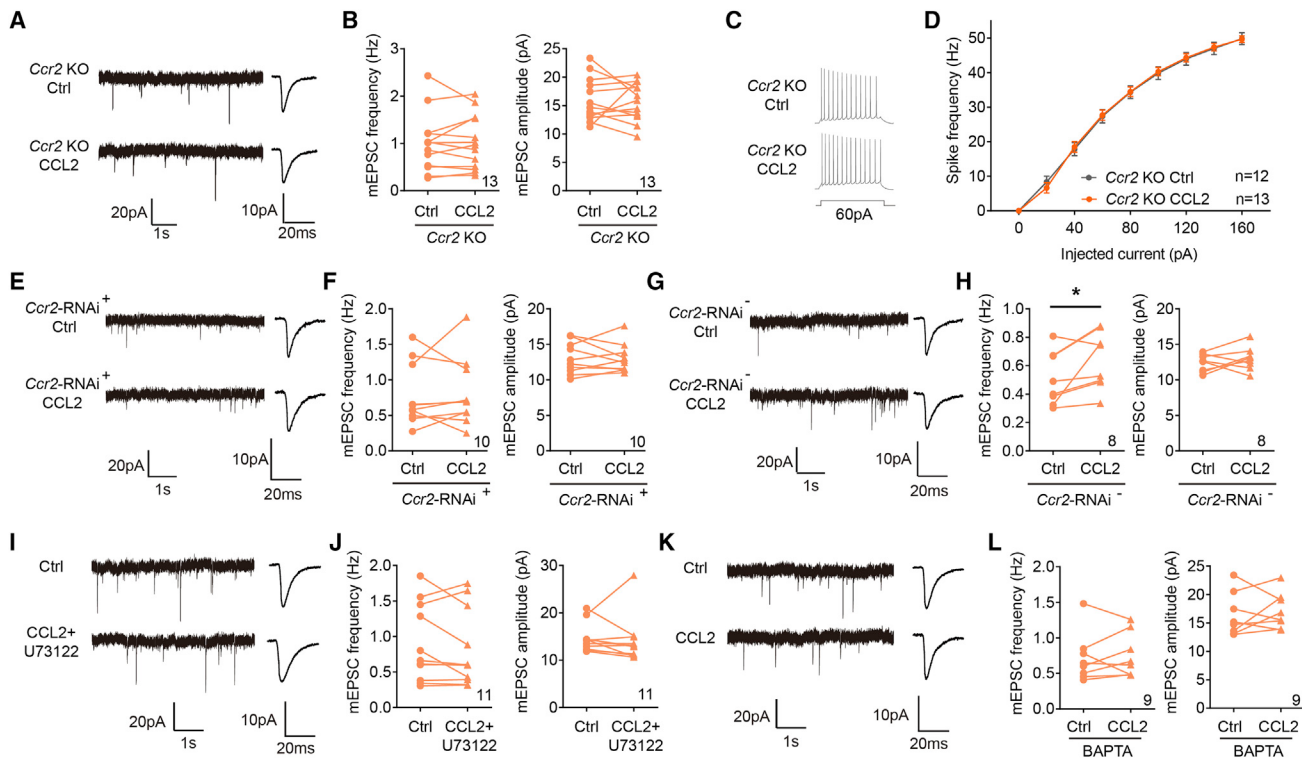


Figure 6. CCL2 Promotes Excitatory Synaptic Transmission through CCR2 and PLC Signaling

(A and B) The effect of CCL2 application on mEPSC frequency and amplitude in CA1 pyramidal neurons of *Ccr2* KO mice, representative traces (A) and summary data (B) (13 cells from 3 mice; Wilcoxon matched-pairs signed rank test).

(C and D) The effect of CCL2 application on firing responses to stepwise current injections in CA1 pyramidal neurons of *Ccr2* KO mice, representative traces (C) and summary data (D) (12–13 cells from 2 mice; two-way ANOVA, Bonferroni post hoc test).

(E–H) mEPSC recordings from Lenti-*Ccr2* RNAi infected CA1 pyramidal neurons (E and F), or neighboring uninfected neurons (G and H) before and after CCL2 application, representative traces (E, G) and summary data (F, H) (8–10 cells from 5 mice per condition; Wilcoxon matched-pairs signed rank test).

(I–L) mEPSC recordings before and after CCL2 application with 10 μ M U73122 in aCSF (I and J) or with 5 mM BAPTA tetracesium in the internal cellular solution (K and L), representative traces (I, K) and summary data (J, L) (9–11 cells from 3 mice; Wilcoxon matched-pairs signed rank test).

See also Figure S7.

frequency, as compared to littermates (Figures 8E and 8F), while their total neuronal excitability exhibited a trend toward reduction (Figures 8G and 8H). When the latency to first spike was analyzed, significant reduction was observed in conditional knockout mice (Figures 8I and 8J), suggesting reduced excitability of these neurons. Consistent with the electrophysiological results, LPS-induced increase in AMPA receptor subunit GluA1 (Figures 8K, 8L, S7P, and S7Q) was substantially attenuated in *Pdgfrb-Cre;Ccl2^{fl/fl}* mice in both the hippocampus and the cerebral cortex (Figures 8M, 8N, S7R, and S7S).

While *Ccl2* mRNA and CCL2 protein levels were significantly reduced in *Pdgfrb-Cre;Ccl2^{fl/fl}* mice following LPS injection (Figures 4D–4F), *Tnf α* , *Il1 β* , and *Il6* mRNA levels were not significantly affected (Figure 8O), providing further evidence that CCL2 is the critical factor secreted by PDGFR β cells to regulate excitatory synaptic transmission.

PDGFR β Cells and CCL2 Mediate Early Neuroinflammatory Response in Adult Mice

The above experiments were carried out in developing mice of approximately P14. To investigate whether our observa-

tions represented a general neuroinflammatory response, we repeated the key experiments in adult (P50–P60) or aged mice (older than P200). *Ccl2* mRNA and CCL2 protein levels were upregulated in PDGFR β cells in both adult and aged mice 2 hr after LPS injection (Figures S10A–S10F). Importantly, CCL2 application significantly increased mEPSC frequency in adult mice (Figures S10G and S10H). The bigger brains of adult mice also allowed us to examine the time course of changes in CCL2 level in the CSF. CCL2 was significantly elevated 2 hr following LPS injection and remained elevated until 24 hr (Figure S10I), consistent with the high level of CCL2 reported in encephalitis patients (Kothur et al., 2016). A significant number of white blood cells (WBC) were only detected 24 hr following LPS injection and not at the earlier 2 hr or 12 hr time point (Figure S10J), suggesting that the upregulation of neuronal activity by PDGFR β -secreted CCL2 occurred prior to significant changes in BBB permeability and that infiltrating WBCs are unlikely to be the main source of CCL2 during early inflammation. Consistently, intravenous injection of Evans blue, a standard assay for measuring BBB permeability (Wang et al., 2004), showed no significant change in the amount of Evans blue leaking to the brain

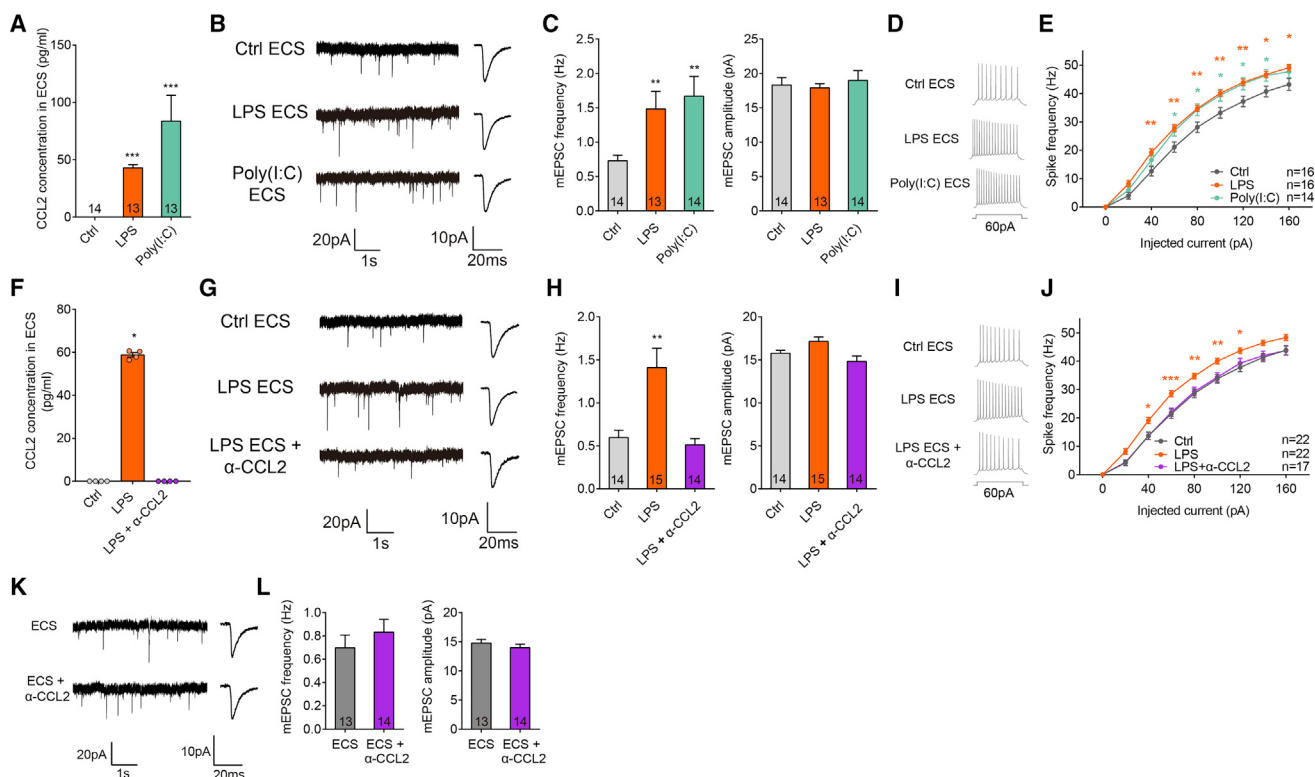


Figure 7. LPS- or Poly(I:C)-Treated HBVP Extracellular Solution Increases Excitatory Synaptic Transmission and Neuronal Excitability in a CCL2-Dependent Manner

(A) Concentration of CCL2 in HBVP extracellular solution (ECS) after LPS or Poly(I:C) treatment (13–14 independent samples per condition; Kruskal-Wallis test, Dunn's post hoc test).

(B and C) The effect of Ctrl ECS, LPS-treated ECS, or Poly(I:C)-treated ECS on mEPSC frequency and amplitude of CA1 pyramidal neurons, representative traces (B) and summary data (C) (13–14 cells from 3 mice per group; Kruskal-Wallis test, Dunn's post hoc test).

(D and E) The effect of Ctrl ECS, LPS ECS, or Poly(I:C) ECS on firing responses to stepwise current injections in CA1 pyramidal neurons, representative traces (D) and summary data (E) (14–16 cells from 3 mice; two-way ANOVA, Bonferroni post hoc test).

(F) Concentration of CCL2 in LPS-stimulated ECS after neutralization with human CCL2 antibody (4 independent samples per group; Kruskal-Wallis test, Dunn's post hoc test).

(G and H) The effect of Ctrl ECS, LPS ECS, or human CCL2 antibody neutralized LPS ECS (LPS ECS+ α -CCL2) on mEPSC frequency and amplitude, representative traces (G) and summary data (H) (14–15 cells from 2–4 mice; Kruskal-Wallis test, Dunn's post hoc test).

(I and J) The effect of Ctrl ECS, LPS ECS, or LPS ECS + α -CCL2 on firing responses to stepwise current injections, representative traces (I) and summary data (J) (17–22 cells from 2–4 mice; two-way ANOVA, Bonferroni post hoc test).

(K and L) The effect of saline-treated ECS (ECS) or human CCL2 antibody neutralized saline-treated ECS (ECS + α -CCL2) on mEPSC frequency and amplitude, representative traces (K) and summary data (L) (13–14 cells from 3 mice; Mann-Whitney test).

See also Figures S8 and S9.

parenchyma 2 hr following LPS injection (Figures S10K and S10L). As a positive control, longer treatment consisting of injection of 1 mg/kg LPS for 3 consecutive days significantly increased the amount of leaked Evans blue (Figures S10K and S10L).

DISCUSSION

In summary, we identify *Co1a1* and *Rgs5* subtypes of PDGFR β cells as early sensors of infection in the brain, within 2 hr of initial insult. We further demonstrate that CCL2 secreted by PDGFR β cells functions as a neuromodulator to rapidly upregulate excitatory synaptic transmission and neuronal firing across multiple brain regions. These effects can be induced by LPS and

Poly(I:C), respectively, mimicking bacterial and viral infections, suggesting that PDGFR β cells and CCL2 likely function as general sensors and mediators of neuroinflammation in the brain.

PDGFR β Cells as Early Sensors of Infection in the Brain

For cells in the brain parenchyma, it is important to be shielded as much as possible from external challenges and, at the same time, to be alerted of incoming danger as quickly as possible. By virtue of their location, cellular components of the vasculature, including endothelial cells, pericytes, vascular smooth muscle cells, perivascular macrophages, and perivascular fibroblast-like cells, are attractive candidates for early sensors. Here, we showed that within 2 hr of LPS or Poly(I:C) injection *in vivo*, *Ccl2* colocalized with PDGFR β cells, but not with endothelial

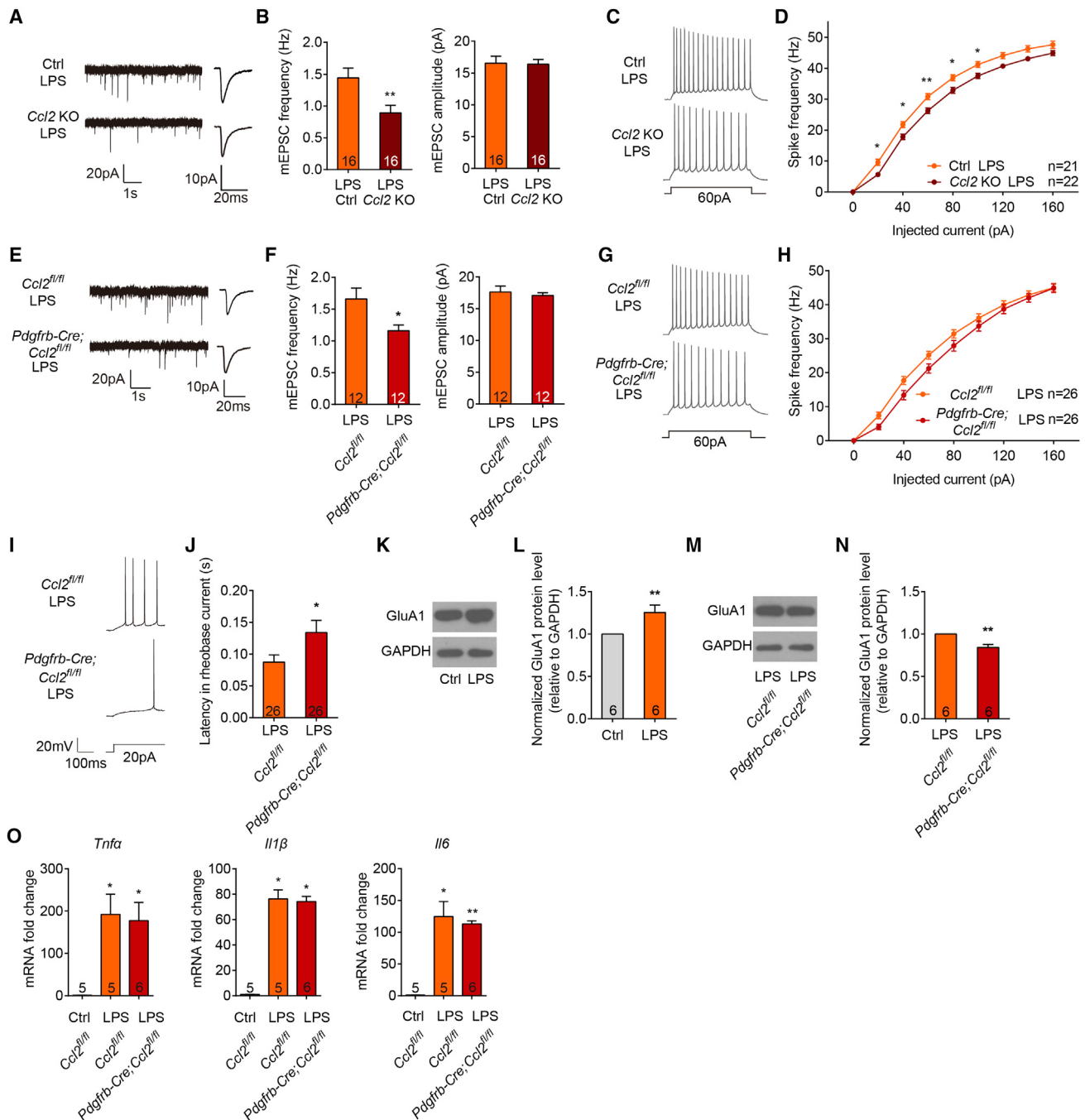


Figure 8. LPS-Induced Enhancement of Excitatory Synaptic Transmission and Neural Excitability Are Attenuated in *Ccl2* Knockout and Pericyte-Specific *Ccl2* Knockout Mice

(A and B) The mEPSC frequency and amplitude of CA1 pyramidal neurons of LPS-injected *Ccl2* knockout mice (*Ccl2* KO LPS) and littermates (LPS Ctrl), representative traces (A) and summary data (B) (16 cells from 4 mice per group; Mann-Whitney test).

(C and D) Firing responses to stepwise current injections of CA1 pyramidal neurons of LPS-injected *Ccl2* KO mice and littermates, representative traces (C) and summary data (D) (21–22 cells from 3 mice per group; two-way ANOVA, Bonferroni post hoc test).

(E and F) The mEPSC frequency and amplitude of CA1 pyramidal neurons of LPS-injected *Pdgfrb-Cre; Ccl2* ^{f/f} mice and littermates, representative traces (E) and summary data (F) (12 cells from 3 mice per group; Mann-Whitney test).

(G and H) Firing responses to stepwise current injections of CA1 pyramidal neurons of LPS-injected *Pdgfrb-Cre; Ccl2* ^{f/f} mice and littermates, representative traces (G) and summary data (H) (26 cells from 4 mice per group; two-way ANOVA, Bonferroni post hoc test).

(I and J) Latency of the first spike induced by rheobase current, calculated from data in (H), representative traces (I) and summary data (J) (Mann-Whitney test).

(legend continued on next page)

cells (Figures 1, 2, 3, 4, S1–S3, S5, and S6). We further used transgenic mice and single-cell RNA-seq to verify their identity (Figures 2, 3, 4, S3, S5, and S6). Importantly, conditional knockout of *Ccl2* using *Pdgfrb-Cre* effectively blocked LPS-induced upregulation of CCL2 expression, while *Ccl2* removal from endothelial cells using *Tie2-Cre* had no such effects (Figures 4D and 4E). These results clearly demonstrate that PDGFR β cells—and not endothelial cells—are the main source of *Ccl2* during early neuroinflammation. They also provide the first *in vivo* evidence for PDGFR β cells as critical mediators of neuroinflammation.

PDGFR β cells comprise mostly pericytes and vascular smooth muscle cells. Our single-cell RNA-seq results showed that *Ccl2* was most highly induced in *Col1a1* and *Rgs5* cell clusters, both of which express *Pdgfrb*, as well as a number of other previously identified pericyte markers, including *Vtn*, *Ifitm1*, and *Tbx18* (Figure 3C). We confirmed colocalization between *Vtn* and *Ccl2* using *in situ* hybridization (Figure 4A). Given the debate regarding the definition of pericytes (Armulik et al., 2011; Attwell et al., 2016), we closely examined these groups. *Rgs5* cells expressed a number of genes identified to be specific to pericytes in a recent single-cell RNA-seq study of the brain vasculature (Vanlandewijck et al., 2018). On further analysis, they could be divided into *Rgs5*(A) cells, which highly express pericyte markers *Abcc9* and *Kcnj8*, as well as *Ccl2*, and *Rgs5*(B) cells, which highly express the smooth muscle cell marker *Acta2* and have low *Ccl2* expression (Figure S6). Consistently, we showed that cultured HBVP—and not HVSMC—expressed high levels of *Ccl2* in response to LPS or Poly(I:C) stimulation (Figure S8). Thus, the subgroup of *Ccl2*-expressing, non-smooth muscle, *Rgs5* cells fit well with cells classically defined as pericytes.

Col1a1 cells have a very similar molecular profile to perivascular fibroblast-like cells, expressing genes including *Col1a1*, *Col1a2*, *Dcn*, *Col3a1*, and *Lum* (Vanlandewijck et al., 2018). Our work independently identified this cell type and, importantly, provided the first *in vivo* evidence of their physiological function. We showed that *Col1a1* cells responded to systemic inflammation by secreting CCL2 as well as some other cytokines. As a chemokine, CCL2 not only regulates neuronal activity, it can also recruit immune cells from the periphery into the brain. In fact, we found a significant number of WBCs in the CSF 24 hr following LPS injection (Figure S10J). LPS-induced increase in WBCs in the CSF was significantly reduced in *Ccr2* knockout mice (Varvel et al., 2016) (data not shown), suggesting a critical role of CCL2 signaling in the recruitment of WBCs to the CNS.

By identifying the *Rgs5* and *Col1a1* subtypes of PDGFR β cells as important early sensors of infection, we do not exclude the contribution of other cell types. Recent work showed that epithelial cells and endothelial cells responded to viral-stimulated, peripheral-secreted interferon β signaling 24 hr post infection (Blank et al., 2016). Of the cytokines and enzymes shown to be induced along blood vessels during early infection, our dataset

showed that *Cxcl10*, *Ptgs2/Cox2*, and *Ptges* are expressed in *Col1a1* cells, *Rgs5* cells, and endothelial cells. Thus, there are at least three combinations of cell-type-specific expression of cytokines and chemokines following infection: PDGFR β cells, endothelial cells, or both. *Rgs5* and *Col1a1* subtypes of PDGFR β cells may also separately express genes, further increasing the complexity.

Both PDGFR β and endothelial cells have access to the circulation and the brain parenchyma. However, endothelial cells, likely due to their polarized nature, have been shown to preferably release cytokines into the circulation (Quan, 2014; Verma et al., 2006). This opens up the hypothesis that PDGFR β may primarily release factors into the brain parenchyma. Especially of interest are *Col1a1*-expressing perivascular fibroblast-like cells, which are located within the perivascular Virchow-Robin space and are implicated in fluid exchange between the brain and the CSF (Iliff et al., 2012; Vanlandewijck et al., 2018). A previous study showed that removal of *Ptgs2* in endothelial cells did not affect the CSF PGE₂ level (Eskilsson et al., 2017). This could be due to high expression of *Ptgs2* also in *Col1a1* and *Rgs5* cells. Whether its expression in *Col1a1* or *Rgs5* cells—or, more generally, in PDGFR β cells—is critical for entry into the CSF is a question for further investigation, with important physiological and clinical significance.

CCL2 Secreted by PDGFR β Cells Relays

Neuroinflammatory Signal to Neurons

Given the close proximity between neurons and blood microvessels (8–23 μ m) (Lovick et al., 1999), perivascular cells are well suited to signal rapidly to and from neurons. Previous work has shown that pericytes, and/or other vascular mural cells, respond to glutamate release from neurons and astrocytes to mediate activity-induced increase in local blood flow (Attwell et al., 2010; Hall et al., 2014; Hill et al., 2015; Iadecola, 2017; Peppiatt et al., 2006; Petzold and Murthy, 2011), an important physiological response to systemic inflammation. However, it was unknown what signal elevated neuronal activity. Here we showed that PDGFR β cells secreted CCL2, which in turn rapidly upregulated excitatory synaptic transmission and total neuronal excitability in glutamatergic neurons from multiple brain regions (Figures 5, 6, 7, and S7). The effect of CCL2 on promoting excitatory synaptic transmission is consistent with previous reports in hippocampal CA1 pyramidal neurons or spinal cord lamina II neurons (Gao et al., 2009; Zhou et al., 2011). Importantly, we showed that LPS-induced enhancement of excitatory synaptic transmission was largely attenuated in *Pdgfrb-Cre;Ccl2^{fl/fl}* mice (Figure 8), suggesting that CCL2 secreted by PDGFR β cells is the main regulator of excitatory synaptic transmission during early systemic inflammation. In other words, PDGFR β cells initiate the cascade of events that lead to increased blood flow, a critical step for mounting early and effective response to external insults.

(K–N) Representative immunoblots (K and M) and quantitation (L and N) of GluA1 levels from membrane fractions of hippocampi of Ctrl and LPS-treated mice (K and L) or LPS-treated *Pdgfrb-Cre;Ccl2^{fl/fl}* mice and littermates (6 mice per group; Mann-Whitney test).

(O) mRNA level of cytokines in *Pdgfrb-Cre;Ccl2^{fl/fl}* mice and littermates; conditions as indicated (5–6 mice per group; Kruskal-Wallis test, Dunn's post hoc test). See Figures S7 and S10.

PDGFR β Cells and Their Subtypes as Gatekeepers

Our results showed that PDGFR β cells, activated during the early phase of systemic inflammation, function as early sensors and responders of neuroinflammation. Other cells, including astrocytes and microglia, are activated later and likely remain activated for the duration of the neuroinflammatory response. Chronic, low-level activation of microglia and astrocytes, likely as a consequence of previous infection and neuroinflammation, is associated with developmental neurological disorders, including intellectual disability, epilepsy, autism spectrum disorder, and schizophrenia (Chandran et al., 2011; Estes and McAllister, 2015, 2016; Klein et al., 2017; Knuesel et al., 2014; Meyer et al., 2011; Vezzani et al., 2011; Xanthos and Sandkühler, 2014).

Effective treatment requires a balance between sufficient immune response to eliminate the infectious agents and not harming the self because of overreaction. The accessibility of PDGFR β cells (and/or *Col1a1*, *Rgs5* subtypes) to the circulatory system and CSF and their early responsiveness, together with their ability to signal widely within the brain parenchyma, make them attractive therapeutic targets. Future studies are required to determine the relative contributions of PDGFR β cells (and/or *Col1a1*, *Rgs5* subtypes), endothelial cells, astrocytes, microglia, and other cell types participating in the neuroinflammatory response as well as their potential therapeutic implications during early and chronic phases of disease.

Although our experiments were mostly performed in developing mice, the main findings, including LPS-induced PDGFR β cells expression of CCL2 and the ability of CCL2 to upregulate excitatory synaptic transmission, also occurred in adult and aging mice (Figure S10). These results suggest that the ability of PDGFR β cells to sense and relay the inflammatory response is a general physiological response that occurs throughout the lifetime of the organism.

STAR★METHODS

Detailed methods are provided in the online version of this paper and include the following:

- KEY RESOURCES TABLE
- CONTACT FOR REAGENT AND RESOURCE SHARING
- EXPERIMENTAL MODEL AND SUBJECT DETAILS
 - Animals
- METHOD DETAILS
 - Drug Treatments
 - Real-Time Quantitative PCR
 - Cell Lines and Extracellular Solution Collection
 - Cytokine Measurements
 - *Ccr2* RNAi Virus and *In Vivo* Stereotaxic Viral Injections
 - Cell Culture and Transfection
 - Western Blots
 - Acute Brain Slice Preparation
 - Whole-Cell Recordings
 - Single-Cell RNA Sequencing and Data Processing
 - Immunocytochemistry
 - Fluorescent *In Situ* Hybridization, RNAscope, and Immunohistochemistry

- Image Acquisition and Image Analysis

- Tail Suspension Test

- Blood-Brain Barrier Permeability Test

- QUANTIFICATION AND STATISTICAL ANALYSIS

- DATA AND SOFTWARE AVAILABILITY

SUPPLEMENTAL INFORMATION

Supplemental Information includes ten figures and two tables and can be found with this article online at <https://doi.org/10.1016/j.neuron.2018.08.030>.

ACKNOWLEDGMENTS

We thank Dr. Volkhard Lindner and Dr. Jiawei Zhou for transgenic mice. We thank Shajin Huang and Yuan Lu for excellent technical assistance. We thank the lab of Xiaohong Xu for advice on *in situ* hybridization. We thank the ION Optical Imaging Facility, Molecular and Cellular Biology Core Facility, and Animal Facility for technical support. We are grateful to Dr. Bin Zhou, Dr. Hongyan Wang, colleagues at ION, and members of the Yu laboratory for suggestions and comments. This work was supported by grants from the National Key R&D Program of China (2016YFA0501000), the National Natural Science Foundation of China (31530030), and the Program of Shanghai Subject Chief Scientist (16XD1404800).

AUTHOR CONTRIBUTIONS

L.D., X.-D.Z., and X.Y. conceived experiments; X.-D.Z. performed electrophysiology experiments with help from H.Y. and G.L.; L.D. and W.-Y.M. performed *in situ* hybridization experiments; L.D. performed all other experiments, with help from W.-Y.M., G.X., Y.-J.S., Q.W., P.Y., Y.W., H.L. and M.Z.; L.D. analyzed single-cell RNA-seq data; L.D., X.-D.Z., and W.-Y.M. analyzed all other data; L.-Y.H., X.T., and W.-H.Z. provided reagents, expertise, and feedback; L.D., X.-D.Z., and X.Y. wrote the manuscript. All authors read, revised, and approved the manuscript.

DECLARATION OF INTERESTS

The authors declare no competing interests.

Received: November 6, 2017

Revised: March 30, 2018

Accepted: August 20, 2018

Published: September 27, 2018

SUPPORTING CITATIONS

The following references appear in the Supplemental Information: Alcendor et al. (2012); Arima et al. (2012); Caruso et al. (2015); Chiang et al. (2013); Favares et al. (2007); Lee et al. (2014); Lewis et al. (2008); Meusel and Imani (2003); Pakala et al. (2010); Qian et al. (2011); Zhang et al. (2009).

REFERENCES

- Ajami, B., Samusik, N., Wieghofer, P., Ho, P.P., Crotti, A., Bjornson, Z., Prinz, M., Fanti, W.J., Nolan, G.P., and Steinman, L. (2018). Single-cell mass cytometry reveals distinct populations of brain myeloid cells in mouse neuroinflammation and neurodegeneration models. *Nat. Neurosci.* 21, 541–551.
- Alcendor, D.J., Charest, A.M., Zhu, W.Q., Vigil, H.E., and Knobel, S.M. (2012). Infection and upregulation of proinflammatory cytokines in human brain vascular pericytes by human cytomegalovirus. *J. Neuroinflammation* 9, 95.
- Arima, Y., Harada, M., Kamimura, D., Park, J.H., Kawano, F., Yull, F.E., Kawamoto, T., Iwakura, Y., Betz, U.A., Márquez, G., et al. (2012). Regional neural activation defines a gateway for autoreactive T cells to cross the blood-brain barrier. *Cell* 148, 447–457.

- Armulik, A., Genové, G., Mäe, M., Nisancioglu, M.H., Wallgard, E., Niaudet, C., He, L., Norlin, J., Lindblom, P., Strittmatter, K., et al. (2010). Pericytes regulate the blood-brain barrier. *Nature* **468**, 557–561.
- Armulik, A., Genové, G., and Betsholtz, C. (2011). Pericytes: developmental, physiological, and pathological perspectives, problems, and promises. *Dev. Cell* **21**, 193–215.
- Attwell, D., Buchan, A.M., Charpak, S., Lauritzen, M., Macvicar, B.A., and Newman, E.A. (2010). Glial and neuronal control of brain blood flow. *Nature* **468**, 232–243.
- Attwell, D., Mishra, A., Hall, C.N., O'Farrell, F.M., and Dalkara, T. (2016). What is a pericyte? *J. Cereb. Blood Flow Metab.* **36**, 451–455.
- Becher, B., Spath, S., and Goverman, J. (2017). Cytokine networks in neuro-inflammation. *Nat. Rev. Immunol.* **17**, 49–59.
- Bell, R.D., Winkler, E.A., Sagare, A.P., Singh, I., LaRue, B., Deane, R., and Zlokovic, B.V. (2010). Pericytes control key neurovascular functions and neuronal phenotype in the adult brain and during brain aging. *Neuron* **68**, 409–427.
- Bifari, F., Decimo, I., Pino, A., Llorens-Bobadilla, E., Zhao, S., Lange, C., Panuccio, G., Boeckx, B., Thienpont, B., Vinckier, S., et al. (2017). Neurogenic radial glia-like cells in meninges migrate and differentiate into functionally integrated neurons in the neonatal cortex. *Cell Stem Cell* **20**, 360–373.e7.
- Blank, T., Detje, C.N., Spieß, A., Hagemeyer, N., Bredecke, S.M., Wolfart, J., Staszewski, O., Zöller, T., Papageorgiou, I., Schneider, J., et al. (2016). Brain endothelial- and epithelial-specific interferon receptor chain 1 drives virus-induced sickness behavior and cognitive impairment. *Immunity* **44**, 901–912.
- Boring, L., Gosling, J., Chensue, S.W., Kunkel, S.L., Farese, R.V., Jr., Broxmeyer, H.E., and Charo, I.F. (1997). Impaired monocyte migration and reduced type 1 (Th1) cytokine responses in C-C chemokine receptor 2 knockout mice. *J. Clin. Invest.* **100**, 2552–2561.
- Boulanger, L.M. (2009). Immune proteins in brain development and synaptic plasticity. *Neuron* **64**, 93–109.
- Breder, C.D., Hazuka, C., Ghayur, T., Klug, C., Huginin, M., Yasuda, K., Teng, M., and Saper, C.B. (1994). Regional induction of tumor necrosis factor alpha expression in the mouse brain after systemic lipopolysaccharide administration. *Proc. Natl. Acad. Sci. USA* **91**, 11393–11397.
- Butler, A., Hoffman, P., Smibert, P., Papalexi, E., and Satija, R. (2018). Integrating single-cell transcriptomic data across different conditions, technologies, and species. *Nat. Biotechnol.* **36**, 411–420.
- Cao, C., Matsumura, K., Yamagata, K., and Watanabe, Y. (1995). Induction by lipopolysaccharide of cyclooxygenase-2 mRNA in rat brain; its possible role in the febrile response. *Brain Res.* **697**, 187–196.
- Caruso, J.A., Akli, S., Pageon, L., Hunt, K.K., and Keyomarsi, K. (2015). The serine protease inhibitor elafin maintains normal growth control by opposing the mitogenic effects of neutrophil elastase. *Oncogene* **34**, 3556–3567.
- Chandran, A., Herbert, H., Misurski, D., and Santosh, M. (2011). Long-term sequelae of childhood bacterial meningitis: an underappreciated problem. *Pediatr. Infect. Dis. J.* **30**, 3–6.
- Chiang, M.F., Yang, S.Y., Lin, I.Y., Hong, J.B., Lin, S.J., Ying, H.Y., Chen, C.M., Wu, S.Y., Liu, F.T., and Lin, K.I. (2013). Inducible deletion of the Blimp-1 gene in adult epidermis causes granulocyte-dominated chronic skin inflammation in mice. *Proc. Natl. Acad. Sci. USA* **110**, 6476–6481.
- Cuttler, A.S., LeClair, R.J., Stohn, J.P., Wang, Q., Sorenson, C.M., Liaw, L., and Lindner, V. (2011). Characterization of Pdgfrb-Cre transgenic mice reveals reduction of ROSA26 reporter activity in remodeling arteries. *Genesis* **49**, 673–680.
- Daneman, R., Zhou, L., Kebede, A.A., and Barres, B.A. (2010). Pericytes are required for blood-brain barrier integrity during embryogenesis. *Nature* **468**, 562–566.
- Dantzer, R., O'Connor, J.C., Freund, G.G., Johnson, R.W., and Kelley, K.W. (2008). From inflammation to sickness and depression: when the immune system subjugates the brain. *Nat. Rev. Neurosci.* **9**, 46–56.
- Deverman, B.E., and Patterson, P.H. (2009). Cytokines and CNS development. *Neuron* **64**, 61–78.
- Ek, M., Engblom, D., Saha, S., Blomqvist, A., Jakobsson, P.J., and Ericsson-Dahlstrand, A. (2001). Inflammatory response: pathway across the blood-brain barrier. *Nature* **410**, 430–431.
- Erickson, M.A., and Banks, W.A. (2011). Cytokine and chemokine responses in serum and brain after single and repeated injections of lipopolysaccharide: multiplex quantification with path analysis. *Brain Behav. Immun.* **25**, 1637–1648.
- Ericsson, A., Liu, C., Hart, R.P., and Sawchenko, P.E. (1995). Type 1 interleukin-1 receptor in the rat brain: distribution, regulation, and relationship to sites of IL-1-induced cellular activation. *J. Comp. Neurol.* **361**, 681–698.
- Eskilsson, A., Matsuwaki, T., Shionoya, K., Mirrasekhian, E., Zajdel, J., Schwaninger, M., Engblom, D., and Blomqvist, A. (2017). Immune-induced fever is dependent on local but not generalized prostaglandin E₂ synthesis in the brain. *J. Neurosci.* **37**, 5035–5044.
- Estes, M.L., and McAllister, A.K. (2015). Immune mediators in the brain and peripheral tissues in autism spectrum disorder. *Nat. Rev. Neurosci.* **16**, 469–486.
- Estes, M.L., and McAllister, A.K. (2016). Maternal immune activation: implications for neuropsychiatric disorders. *Science* **353**, 772–777.
- Favrais, G., Schwendimann, L., Gressens, P., and Lelièvre, V. (2007). Cyclooxygenase-2 mediates the sensitizing effects of systemic IL-1-beta on excitotoxic brain lesions in newborn mice. *Neurobiol. Dis.* **25**, 496–505.
- Gaengel, K., Genové, G., Armulik, A., and Betsholtz, C. (2009). Endothelial-mural cell signaling in vascular development and angiogenesis. *Arterioscler. Thromb. Vasc. Biol.* **29**, 630–638.
- Gao, Y.J., Zhang, L., Samad, O.A., Suter, M.R., Yasuhiko, K., Xu, Z.Z., Park, J.Y., Lind, A.L., Ma, Q., and Ji, R.R. (2009). JNK-induced MCP-1 production in spinal cord astrocytes contributes to central sensitization and neuropathic pain. *J. Neurosci.* **29**, 4096–4108.
- Gosselin, R.D., Varela, C., Banisadr, G., Mechighel, P., Rostene, W., Kitabgi, P., and Melik-Parsadaniantz, S. (2005). Constitutive expression of CCR2 chemokine receptor and inhibition by MCP-1/CCL2 of GABA-induced currents in spinal cord neurones. *J. Neurochem.* **95**, 1023–1034.
- Hall, C.N., Reynell, C., Gesslein, B., Hamilton, N.B., Mishra, A., Sutherland, B.A., O'Farrell, F.M., Buchan, A.M., Lauritzen, M., and Attwell, D. (2014). Capillary pericytes regulate cerebral blood flow in health and disease. *Nature* **508**, 55–60.
- Hartmann, D.A., Underly, R.G., Grant, R.I., Watson, A.N., Lindner, V., and Shih, A.Y. (2015). Pericyte structure and distribution in the cerebral cortex revealed by high-resolution imaging of transgenic mice. *Neurophotonics* **2**, 041402.
- He, L., Vanlandewijck, M., Raschperger, E., Andaloussi Mäe, M., Jung, B., Lebouvier, T., Ando, K., Hofmann, J., Keller, A., and Betsholtz, C. (2016). Analysis of the brain mural cell transcriptome. *Sci. Rep.* **6**, 35108.
- Hill, R.A., Tong, L., Yuan, P., Murikinati, S., Gupta, S., and Grutzendler, J. (2015). Regional blood flow in the normal and ischemic brain is controlled by arteriolar smooth muscle cell contractility and not by capillary pericytes. *Neuron* **87**, 95–110.
- Iadecola, C. (2017). The neurovascular unit coming of age: a journey through neurovascular coupling in health and disease. *Neuron* **96**, 17–42.
- Iliff, J.J., Wang, M., Liao, Y., Plogg, B.A., Peng, W., Gundersen, G.A., Benveniste, H., Vates, G.E., Deane, R., Goldman, S.A., et al. (2012). A paravascular pathway facilitates CSF flow through the brain parenchyma and the clearance of interstitial solutes, including amyloid β. *Sci. Transl. Med.* **4**, 147ra111.
- Jung, B., Arnold, T.D., Raschperger, E., Gaengel, K., and Betsholtz, C. (2018). Visualization of vascular mural cells in developing brain using genetically labeled transgenic reporter mice. *J. Cereb. Blood Flow Metab.* **38**, 456–468.
- Juszczak, G.R., Sliwa, A.T., Wolak, P., Tymosiak-Zielinska, A., Lisowski, P., and Swiergiel, A.H. (2006). The usage of video analysis system for detection of immobility in the tail suspension test in mice. *Pharmacol. Biochem. Behav.* **85**, 332–338.

- Kawai, T., and Akira, S. (2010). The role of pattern-recognition receptors in innate immunity: update on Toll-like receptors. *Nat. Immunol.* 11, 373–384.
- Klein, R.S., Garber, C., and Howard, N. (2017). Infectious immunity in the central nervous system and brain function. *Nat. Immunol.* 18, 132–141.
- Knuesel, I., Chicha, L., Britschgi, M., Schobel, S.A., Bodmer, M., Hellings, J.A., Toovey, S., and Prinsen, E.P. (2014). Maternal immune activation and abnormal brain development across CNS disorders. *Nat. Rev. Neurol.* 10, 643–660.
- Kobayashi, S., Saito, H., and Okada, M. (1994). A simplified and efficient method for in-situ hybridization to whole *Drosophila* embryos, using electrophoresis for removing non-hybridized probes. *Dev. Growth Differ.* 36, 629–632.
- Koni, P.A., Joshi, S.K., Temann, U.A., Olson, D., Burkly, L., and Flavell, R.A. (2001). Conditional vascular cell adhesion molecule 1 deletion in mice: impaired lymphocyte migration to bone marrow. *J. Exp. Med.* 193, 741–754.
- Kothur, K., Wienholt, L., Brilot, F., and Dale, R.C. (2016). CSF cytokines/chemokines as biomarkers in neuroinflammatory CNS disorders: a systematic review. *Cytokine* 77, 227–237.
- Kuang, Y., Wu, Y., Jiang, H., and Wu, D. (1996). Selective G protein coupling by C-C chemokine receptors. *J. Biol. Chem.* 271, 3975–3978.
- Lee, S.M., Kok, K.H., Jaume, M., Cheung, T.K., Yip, T.F., Lai, J.C., Guan, Y., Webster, R.G., Jin, D.Y., and Peiris, J.S. (2014). Toll-like receptor 10 is involved in induction of innate immune responses to influenza virus infection. *Proc. Natl. Acad. Sci. USA* 111, 3793–3798.
- Leuschner, F., Dutta, P., Gorbatov, R., Novobrantseva, T.I., Donahoe, J.S., Courties, G., Lee, K.M., Kim, J.I., Markmann, J.F., Marinelli, B., et al. (2011). Therapeutic siRNA silencing in inflammatory monocytes in mice. *Nat. Biotechnol.* 29, 1005–1010.
- Lewis, E.C., Mizrahi, M., Toledano, M., Defelice, N., Wright, J.L., Churg, A., Shapiro, L., and Dinarello, C.A. (2008). alpha1-Antitrypsin monotherapy induces immune tolerance during islet allograft transplantation in mice. *Proc. Natl. Acad. Sci. USA* 105, 16236–16241.
- Liddelow, S.A., and Barres, B.A. (2017). Reactive astrocytes: production, function, and therapeutic potential. *Immunity* 46, 957–967.
- Liu, L., and Duff, K. (2008). A technique for serial collection of cerebrospinal fluid from the cisterna magna in mouse. *J. Vis. Exp.* 21, 960.
- Liu, L., Oza, S., Hogan, D., Perin, J., Rudan, I., Lawn, J.E., Cousens, S., Mathers, C., and Black, R.E. (2015). Global, regional, and national causes of child mortality in 2000–13, with projections to inform post-2015 priorities: an updated systematic analysis. *Lancet* 385, 430–440.
- Lovick, T.A., Brown, L.A., and Key, B.J. (1999). Neurovascular relationships in hippocampal slices: physiological and anatomical studies of mechanisms underlying flow-metabolism coupling in intraparenchymal microvessels. *Neuroscience* 92, 47–60.
- Lu, B., Rutledge, B.J., Gu, L., Fiorillo, J., Lukacs, N.W., Kunkel, S.L., North, R., Gerard, C., and Rollins, B.J. (1998). Abnormalities in monocyte recruitment and cytokine expression in monocyte chemoattractant protein 1-deficient mice. *J. Exp. Med.* 187, 601–608.
- Malenka, R.C., and Nicoll, J.A. (1997). Silent synapses speak up. *Neuron* 19, 473–476.
- Meusel, T.R., and Imani, F. (2003). Viral induction of inflammatory cytokines in human epithelial cells follows a p38 mitogen-activated protein kinase-dependent but NF- κ B-independent pathway. *J. Immunol.* 171, 3768–3774.
- Meyer, U., Feldon, J., and Dammann, O. (2011). Schizophrenia and autism: both shared and disorder-specific pathogenesis via perinatal inflammation? *Pediatr. Res.* 69, 26R–33R.
- Miller, R.E., Tran, P.B., Das, R., Ghoreishi-Haack, N., Ren, D., Miller, R.J., and Malfait, A.M. (2012). CCR2 chemokine receptor signaling mediates pain in experimental osteoarthritis. *Proc. Natl. Acad. Sci. USA* 109, 20602–20607.
- Mrdjen, D., Pavlovic, A., Hartmann, F.J., Schreiner, B., Utz, S.G., Leung, B.P., Lelios, I., Heppner, F.L., Kipnis, J., Merkler, D., et al. (2018). High-dimensional single-cell mapping of central nervous system immune cells reveals distinct myeloid subsets in health, aging, and disease. *Immunity* 48, 380–395.e6.
- Nadeau, S., and Rivest, S. (1999). Regulation of the gene encoding tumor necrosis factor alpha (TNF-alpha) in the rat brain and pituitary in response to different models of systemic immune challenge. *J. Neuropathol. Exp. Neurol.* 58, 61–77.
- Nakamori, T., Morimoto, A., Yamaguchi, K., Watanabe, T., and Murakami, N. (1994). Interleukin-1 beta production in the rabbit brain during endotoxin-induced fever. *J. Physiol.* 476, 177–186.
- Norden, D.M., Trojanowski, P.J., Villanueva, E., Navarro, E., and Godbout, J.P. (2016). Sequential activation of microglia and astrocyte cytokine expression precedes increased Iba-1 or GFAP immunoreactivity following systemic immune challenge. *Glia* 64, 300–316.
- Pakala, S.B., Reddy, S.D., Bui-Nguyen, T.M., Rangaraju, S.S., Bommane, A., and Kumar, R. (2010). MTA1 coregulator regulates LPS response via MyD88-dependent signaling. *J. Biol. Chem.* 285, 32787–32792.
- Peng, Y.R., Zeng, S.Y., Song, H.L., Li, M.Y., Yamada, M.K., and Yu, X. (2010). Postsynaptic spiking homeostatically induces cell-autonomous regulation of inhibitory inputs via retrograde signaling. *J. Neurosci.* 30, 16220–16231.
- Peppiatt, C.M., Howarth, C., Mobbs, P., and Attwell, D. (2006). Bidirectional control of CNS capillary diameter by pericytes. *Nature* 443, 700–704.
- Petzold, G.C., and Murthy, V.N. (2011). Role of astrocytes in neurovascular coupling. *Neuron* 71, 782–797.
- Prinz, M., and Priller, J. (2014). Microglia and brain macrophages in the molecular age: from origin to neuropsychiatric disease. *Nat. Rev. Neurosci.* 15, 300–312.
- Prinz, M., and Priller, J. (2017). The role of peripheral immune cells in the CNS in steady state and disease. *Nat. Neurosci.* 20, 136–144.
- Qian, B.Z., Li, J., Zhang, H., Kitamura, T., Zhang, J., Campion, L.R., Kaiser, E.A., Snyder, L.A., and Pollard, J.W. (2011). CCL2 recruits inflammatory monocytes to facilitate breast-tumour metastasis. *Nature* 475, 222–225.
- Quan, N. (2014). In-depth conversation: spectrum and kinetics of neuroimmune afferent pathways. *Brain Behav. Immun.* 40, 1–8.
- Quan, N., Whiteside, M., and Herkenham, M. (1998a). Cyclooxygenase 2 mRNA expression in rat brain after peripheral injection of lipopolysaccharide. *Brain Res.* 802, 189–197.
- Quan, N., Whiteside, M., and Herkenham, M. (1998b). Time course and localization patterns of interleukin-1beta messenger RNA expression in brain and pituitary after peripheral administration of lipopolysaccharide. *Neuroscience* 83, 281–293.
- Réaux-Le Goazigo, A., Van Steenwinckel, J., Rostène, W., and Mélik-Parsadanian, S. (2013). Current status of chemokines in the adult CNS. *Prog. Neurobiol.* 104, 67–92.
- Rustenhoven, J., Jansson, D., Smyth, L.C., and Dragunow, M. (2017). Brain pericytes as mediators of neuroinflammation. *Trends Pharmacol. Sci.* 38, 291–304.
- Saijo, K., and Glass, C.K. (2011). Microglial cell origin and phenotypes in health and disease. *Nat. Rev. Immunol.* 11, 775–787.
- Salter, M.W., and Stevens, B. (2017). Microglia emerge as central players in brain disease. *Nat. Med.* 23, 1018–1027.
- Satija, R., Farrell, J.A., Gennert, D., Schier, A.F., and Regev, A. (2015). Spatial reconstruction of single-cell gene expression data. *Nat. Biotechnol.* 33, 495–502.
- Shatz, C.J. (2009). MHC class I: an unexpected role in neuronal plasticity. *Neuron* 64, 40–45.
- Shi, C., Jia, T., Mendez-Ferrer, S., Hohl, T.M., Serbina, N.V., Lipuma, L., Leiner, I., Li, M.O., Frenette, P.S., and Pamer, E.G. (2011). Bone marrow mesenchymal stem and progenitor cells induce monocyte emigration in response to circulating toll-like receptor ligands. *Immunity* 34, 590–601.
- Sofroniew, M.V. (2015). Astrocyte barriers to neurotoxic inflammation. *Nat. Rev. Neurosci.* 16, 249–263.
- Sweeney, M.D., Ayyadurai, S., and Zlokovic, B.V. (2016). Pericytes of the neurovascular unit: key functions and signaling pathways. *Nat. Neurosci.* 19, 771–783.

- Thibeault, I., Laflamme, N., and Rivest, S. (2001). Regulation of the gene encoding the monocyte chemoattractant protein 1 (MCP-1) in the mouse and rat brain in response to circulating LPS and proinflammatory cytokines. *J. Comp. Neurol.* 434, 461–477.
- Vallières, L., and Rivest, S. (1997). Regulation of the genes encoding interleukin-6, its receptor, and gp130 in the rat brain in response to the immune activator lipopolysaccharide and the proinflammatory cytokine interleukin-1beta. *J. Neurochem.* 69, 1668–1683.
- van Praag, H., Schinder, A.F., Christie, B.R., Toni, N., Palmer, T.D., and Gage, F.H. (2002). Functional neurogenesis in the adult hippocampus. *Nature* 415, 1030–1034.
- Vanlandewijck, M., He, L., Mäe, M.A., Andrae, J., Ando, K., Del Gaudio, F., Nahar, K., Lebouvier, T., Laviña, B., Gouveia, L., et al. (2018). A molecular atlas of cell types and zonation in the brain vasculature. *Nature* 554, 475–480.
- Varvel, N.H., Neher, J.J., Bosch, A., Wang, W., Ransohoff, R.M., Miller, R.J., and Dingledine, R. (2016). Infiltrating monocytes promote brain inflammation and exacerbate neuronal damage after status epilepticus. *Proc. Natl. Acad. Sci. USA* 113, E5665–E5674.
- Verma, S., Nakaoke, R., Dohgu, S., and Banks, W.A. (2006). Release of cytokines by brain endothelial cells: a polarized response to lipopolysaccharide. *Brain Behav. Immun.* 20, 449–455.
- Vezzani, A., French, J., Bartfai, T., and Baram, T.Z. (2011). The role of inflammation in epilepsy. *Nat. Rev. Neurol.* 7, 31–40.
- Wang, T., Town, T., Alexopoulou, L., Anderson, J.F., Fikrig, E., and Flavell, R.A. (2004). Toll-like receptor 3 mediates West Nile virus entry into the brain causing lethal encephalitis. *Nat. Med.* 10, 1366–1373.
- Wohleb, E.S., Franklin, T., Iwata, M., and Duman, R.S. (2016). Integrating neuroimmune systems in the neurobiology of depression. *Nat. Rev. Neurosci.* 17, 497–511.
- Wu, M.V., Manoli, D.S., Fraser, E.J., Coats, J.K., Tollkuhn, J., Honda, S., Harada, N., and Shah, N.M. (2009). Estrogen masculinizes neural pathways and sex-specific behaviors. *Cell* 139, 61–72.
- Xanthos, D.N., and Sandkühler, J. (2014). Neurogenic neuroinflammation: inflammatory CNS reactions in response to neuronal activity. *Nat. Rev. Neurosci.* 15, 43–53.
- Xiu, J., Zhang, Q., Zhou, T., Zhou, T.T., Chen, Y., and Hu, H. (2014). Visualizing an emotional valence map in the limbic forebrain by TAI-FISH. *Nat. Neurosci.* 17, 1552–1559.
- Zeisel, A., Muñoz-Manchado, A.B., Codeluppi, S., Lönnérberg, P., La Manno, G., Juréus, A., Marques, S., Munguba, H., He, L., Betsholtz, C., et al. (2015). Brain structure. Cell types in the mouse cortex and hippocampus revealed by single-cell RNA-seq. *Science* 347, 1138–1142.
- Zhang, J., Rubio, V., Lieberman, M.W., and Shi, Z.Z. (2009). OLA1, an Ogb-like ATPase, suppresses antioxidant response via nontranscriptional mechanisms. *Proc. Natl. Acad. Sci. USA* 106, 15356–15361.
- Zhang, Y., Chen, K., Sloan, S.A., Bennett, M.L., Scholze, A.R., O'Keeffe, S., Phatnani, H.P., Guarneri, P., Caneda, C., Ruderisch, N., et al. (2014). An RNA-sequencing transcriptome and splicing database of glia, neurons, and vascular cells of the cerebral cortex. *J. Neurosci.* 34, 11929–11947.
- Zhao, Z., Nelson, A.R., Betsholtz, C., and Zlokovic, B.V. (2015). Establishment and dysfunction of the blood-brain barrier. *Cell* 163, 1064–1078.
- Zheng, J.J., Li, S.J., Zhang, X.D., Miao, W.Y., Zhang, D., Yao, H., and Yu, X. (2014). Oxytocin mediates early experience-dependent cross-modal plasticity in the sensory cortices. *Nat. Neurosci.* 17, 391–399.
- Zhou, Y., Tang, H., Liu, J., Dong, J., and Xiong, H. (2011). Chemokine CCL2 modulation of neuronal excitability and synaptic transmission in rat hippocampal slices. *J. Neurochem.* 116, 406–414.
- Zlotnik, A., and Yoshie, O. (2012). The chemokine superfamily revisited. *Immunity* 36, 705–716.

STAR★METHODS**KEY RESOURCES TABLE**

REAGENT or RESOURCE	SOURCE	IDENTIFIER
Antibodies		
ICC: Anti-MCP1 antibody	Abcam	Cat# ab9669; RRID: AB_2071551
ICC: NF κ B p65	Santa Cruz	Cat# SC-372; RRID: AB_632037
IHC/ICC: PDGF R beta antibody	R&D Systems	Cat# AF1042; RRID: AB_2162633
IHC: glucose transporter GLUT-1	Millipore	Cat# CBL242; RRID: AB_327046
IHC: glial fibrillary acidic protein (GFAP)	Dako	Cat# Z0334; RRID: AB_10013382
IHC: Iba1	Wako	Cat# 019-19741; RRID: AB_839504
IHC: tdTomato	SICGEN	Cat# AB8181-200; RRID: AB_2722750
IHC: Donkey anti-Rabbit Alexa Fluor 488	Thermo Fisher Scientific	Cat# A21206; RRID: AB_2535792
IHC: Donkey anti-Rabbit Alexa Fluor 568	Thermo Fisher Scientific	Cat# A10042; RRID: AB_2534017
IHC: Donkey anti-Goat Alexa Fluor 488	Thermo Fisher Scientific	Cat# A11055; RRID: AB_2534102
IHC: Donkey anti-Goat Alexa Fluor 568	Thermo Fisher Scientific	Cat# A11057; RRID: AB_2534104
ISH: anti-Digoxigenin-AP Fab fragments	Roche	Cat# 11093274910; RRID: AB_514497
ISH: anti-Digoxigenin-POD Fab fragments	Roche	Cat# 11207733910; RRID: AB_514500
ISH: peroxidase-IgG fraction monoclonal mouse anti-fluorescein	Jackson ImmunoResearch	Cat# 200-032-037; RRID: AB_2314402
ISH: anti-DNP-488	Invitrogen	Cat# A-11097; RRID: AB_2314332
ISH: tyramide signal amplification TSA plus DNP system	PerkinElmer	Cat# NEL747A; RRID: AB_2314317
ISH: tyramide signal amplification (TSA) plus cyanine 3 system	PerkinElmer	Cat# NEL744
WB: GFP	Thermo Fisher Scientific	Cat# A11122; RRID: AB_221569
WB: GluA1	Millipore	Cat# AB1504; RRID: AB_11212863
WB: GAPDH	Kangchen Biotech	Cat# KC-5G4; RRID: AB_2493106
Chromium Single Cell 3' Library & Gel Bead Kit v.2	10x Genomics	Cat# 120237
Chromium i7 Multiplex Kit, 96 rxns	10x Genomics	Cat# 120262
Chromium Single Cell A Chip Kit	10x Genomics	Cat# 120236
RNAscope Multiplex Fluorescent Reagent Kit v.2	Advanced Cell Diagnostics	Cat# 323100
Bacterial and Virus Strains		
<i>E. coli</i> . DH5 α	TIANGEN Biotech	Cat# CB101
Lentiviruses	Genechem, Shanghai, China	N/A
Chemicals, Peptides, and Recombinant Proteins		
Lipopolysaccharides (<i>Escherichia coli</i> , serotype O111:B4)	Sigma	Cat# L2630-25MG
Poly(I:C)	Tocris	Cat# 4287
ODN-1668	InvivoGen	Cat# tlr1-1668-5
DAPI	Thermo Fisher Scientific	Cat# D1306; RRID:AB_2629482
Recombinant Mouse CCL2/JE/MCP-1	R&D Systems	Cat# 479-JE-050
BAPTA tetracesium salt	Thermo Fisher Scientific	Cat# B-1212
NBQX	Tocris	Cat# 1044
D-APV	Tocris	Cat# 0106
Gabazine	Tocris	Cat# 1262
U73122	Tocris	Cat# 1268
Fast red	Roche	Cat# 11496549001

(Continued on next page)

Continued

REAGENT or RESOURCE	SOURCE	IDENTIFIER
Fast red	Sigma	Cat# F4523
Evans blue	Sigma	Cat# E2129-10G
Critical Commercial Assays		
Cytokine/chemokine magnetic bead panel 96-well plate assay	R&D Systems	Cat# MCYTOMAG-70K
Deposited Data		
10× single-cell RNA-seq data	This paper	GEO: GSE112436
Experimental Models: Cell Lines		
Human brain vascular pericytes (HBVP)	ScienCell	Cat# 1200
Human brain vascular smooth muscle cells (HBVSMC)	ScienCell	Cat# 1100
Experimental Models: Organisms/Strains		
Mouse: C57BL/6J	Shanghai Laboratory Animal Center, Chinese Academy of Sciences (Shanghai, China)	N/A
Mouse: <i>Ccl2</i> KO; <i>B6.129S4-Ccl2tm1R0l/J</i>	The Jackson Laboratory	RRID: IMSR_JAX:004434
Mouse: <i>Ccl2-RFP</i> ^{fl/fl} ; <i>B6.Cg-Ccl2tm1.Pame/J</i>	The Jackson Laboratory	RRID: IMSR_JAX:016849
Mouse: <i>Ccr2</i> KO; <i>B6.129S4-Ccr2tm1Ifc/J</i>	The Jackson Laboratory	RRID: IMSR_JAX:004999
Mouse: <i>Ai9</i> ^{fl/fl} ; <i>B6.Cg-Gt(ROSA)26Sor</i> ^{tm9(CAG-tdTomato)Hze/J}	The Jackson Laboratory	RRID: IMSR_JAX:007909
Mouse: <i>TIE2Cre</i> ; <i>B6.Cg-Tg(Tek-cre)12Flv/J</i>	The Jackson Laboratory	RRID: IMSR_JAX:004128
Mouse: <i>Pdgfrb-Cre</i>	Cuttler et al., 2011	N/A
Oligonucleotides		
ISH: CCL2_Probe_1-Forward primer: CCAGCACCAAGCCAACTCT	This paper	N/A
ISH: CCL2_Probe_1-Reverse primer: GGTGTACAAAATAATATAT	This paper	N/A
ISH: CCL2_Probe_2-Forward primer: TCTCACTGAAGCCAGCTCTC	Miller et al., 2012	N/A
ISH: CCL2_Probe_2-Reverse primer: CATCACAGTCCGAGTCACAC	Miller et al., 2012	N/A
ISH: <i>Vtn</i> _Probe_1-Forward primer: TGCGCGACTACATGGAGCA	Allen Brain Atlas, probe: RP_040922_01_C11	N/A
ISH: <i>Vtn</i> _Probe_1-Reverse primer: GCCATAGCAGCGTCCACT	Allen Brain Atlas, probe: RP_040922_01_C11	N/A
RNAscope probe: <i>Ccl2</i>	Advanced Cell Diagnostics	Cat# 311791
RNAscope probe: <i>Col1a1</i>	Advanced Cell Diagnostics	Cat# 319371-C2
Mouse <i>Ccr2</i> shRNA sequence: TGCTAACGTCTCTGCAA	Leuschner et al., 2011	N/A
Software and Algorithms		
Clampfit	Molecular Devices	https://www.moleculardevices.com/products/axon-patch-clamp-system/acquisition-and-analysis-software/pclamp-software-suite
MiniAnalysis	Synaptosoft	http://www.synaptosoft.com/MiniAnalysis/
GraphPad Prism	GraphPad Software	https://www.graphpad.com/scientific-software/prism/
ImageJ	NIH	https://imagej.nih.gov/ij/
Fiji	NIH	http://fiji.sc/
Image-Pro Plus	Media Cybernetics	http://www.mediacy.com/imageproplus

(Continued on next page)

Continued

REAGENT or RESOURCE	SOURCE	IDENTIFIER
R v.3.4.3	R Foundation for Statistical Computing	https://www.r-project.org/
Cell Ranger v.2.1.0	10x Genomics	https://support.10xgenomics.com/single-cell-gene-expression/software/pipelines/latest/what-is-cell-ranger
Seurat v.2.2.1	Satija Lab	https://satijalab.org/seurat/
RStudio	RStudio	https://www.rstudio.com/products/rstudio/

CONTACT FOR REAGENT AND RESOURCE SHARING

Further information and requests for resources and reagents should be directed to and will be fulfilled by the Lead Contact, Xiang Yu (yuxiang@ion.ac.cn).

EXPERIMENTAL MODEL AND SUBJECT DETAILS**Animals**

All animal procedures complied with the animal care standards set forth by the US National Institutes of Health and were approved by the Institutional Animal Care and Use Committee of the Institute of Neuroscience, Chinese Academy of Sciences. Mice were kept on C57BL/6 background and under a 12 h – 12 h light-dark cycle with food and water provided ad libitum from the cage lid.

Ccl2 knockout mice (*Ccl2* KO; *B6.129S4-Ccl2^{tm1R0j}*/J; JAX strain 004434 | *Ccl2* KO) ([Lu et al., 1998](#)), *Ccl2* floxed mice (*B6.Cg-Ccl2^{tm1.1Pame}*/J; JAX strain 016849 | *Ccl2-RFP^{flx}*) ([Shi et al., 2011](#)), *Ccr2* knockout mice (*Ccr2* KO; *B6.129S4-Ccr2^{tm1fbc}*/J; JAX strain 004999 | *Ccr2* KO) ([Boring et al., 1997](#)), Ai9 mice (*B6.Cg-Gt(ROSA)26Sor^{tm9(CAG-tdTomato)Hze}*/J; JAX strain 007909| *Ai9^{flx}*), and *Tie2-Cre* mice (*B6.Cg-Tg(Tek-cre)12Flv*/J; JAX strain 004128 | *TIE2Cre*) were from the Jackson Laboratory (Bar Harbor, ME, USA). *Ccl2-RFP^{flx}* mice contain loxP sites flanking exons 2–3 of *Ccl2*, as well as an HA peptide followed by an aphthovirus 2A cleavage site and a cleavable red fluorescent protein (RFP) at the 3' end of exon 3 ([Shi et al., 2011](#)). Fluorescence is seen in all *Ccl2*-expressing cells. When these mutant mice are bred to Cre mice, resulting offspring will have exons 2–3 of *Ccl2*, as well as RFP, deleted in the Cre-expressing tissue. *Tie2-Cre* expresses Cre recombinase under the receptor tyrosine kinase Tek promoter/enhancer and has been shown to be uniformly expressed in endothelial cells ([Koni et al., 2001](#)).

Pdgfrb-Cre is a transgenic line expressing Cre recombinase under control of the platelet-derived growth factor receptor-beta *Pdgfrb* promoter sequence (−4.7/+0.1 kb, originally named Tg(*Pdgfrb-Cre*)^{35VII}), obtained from Dr. Jiawei Zhou (Institute of Neuroscience, Chinese Academy of Sciences, Shanghai, China), with permission from Dr. Volkhard Lindner (Maine Medical Center, Scarborough, ME, USA) ([Cuttler et al., 2011](#)).

Mice were maintained on C57BL/6 background. Male heterozygous *Pdgfrb-Cre* or *Tie2-Cre* mice were bred with female Ai9 reporter mice or *Ccl2* floxed mice. The experimental group consisted of mice homozygous for loxP and heterozygous for Cre, while the control group consisted of homozygous loxP littermates. For Ai9 experiments, heterozygous mice were used. Both male and female mice were used in all experiments. The P14 group consisted of P14–P16 mice. P14 mice were used, except for data presented in [Figures 4F](#) and [S10](#), where adult mice (P50 – P60) or aged mice (older than P200) were used. The number of mice used is as indicated in figure legends; 3 or more mice were used per experimental condition.

METHOD DETAILS**Drug Treatments**

Mice were intraperitoneally injected with a single dose of lipopolysaccharides (*Escherichia coli*, serotype O111:B4, Sigma, Cat# L2630-25MG; 10 mg/kg), Poly(I:C) (Tocris, Cat# 4287; 10 mg/kg), or ODN-1668 (InvivoGen, San Diego, CA, USA; Cat# tlr1-1668-5; 10 mg/kg), unless otherwise stated. Control animals received the same volume of saline. Mice were sacrificed at specific time points post-injection as described.

Real-Time Quantitative PCR

Total RNA was extracted from tissue (whole hippocampus) or cultured cell samples using TRIzol reagent (Invitrogen, Cat# 15596018). First-strand cDNA was generated using the M-MLV reverse transcriptase (Promega, Cat# M1701) according to the manufacturer's protocols. Primers are as listed in [Table S2](#). Human primers were used for HBVP and HBVSMC samples.

Real-time quantitative PCR (qPCR) was performed using SYBR Green Master Mix (TaKaRa, Cat# RR420A) on LightCycler 480 (Roche Applied Science). All reactions were carried out in duplicates, and the comparative C_T method was used for comparisons between samples unless otherwise stated.

For absolute quantification, DNA fragments were cloned into pMD18-T Vector (TaKaRa, Cat# 6013) using the above primers. Six 10-fold dilutions of the resulting plasmids were used to generate the standard curve, from which absolute copy numbers were calculated.

Cell Lines and Extracellular Solution Collection

Human brain vascular pericytes (HBVP; ScienCell, Cat# 1200) were maintained in pericyte medium (ScienCell, Cat# 1201). Human brain vascular smooth muscle cells (HBVSMC; ScienCell, Cat# 1100) were maintained in smooth muscle cell medium (ScienCell, Cat# 1101). It is unknown if HBVP and HBVSMC are of male or female origin. Cells were used between passages 2 to 5. Saline (0.9% NaCl; Ctrl), 10 µg/ml LPS or 10 µg/ml Poly(I:C) in pericyte medium was used to stimulate HBVP for 1 - 4 h, as indicated. For extracellular solution (ECS) collection, 2 h after stimulation, the medium were fully washed twice in ECS, and incubated with fresh ECS for 4 h before collection. For the antibody neutralization experiment, human CCL2 antibody (R&D Systems, Cat# MAB679-500, 1:100) were added to the ECS and incubated at 37°C for 2 h before experiments. ECS contained (in mM): 129 NaCl, 5 KCl, 1 MgCl₂, 2 CaCl₂, 25 HEPES and 30 D-glucose (pH 7.3, 310 mOsm).

Cytokine Measurements

Brain tissues were homogenized in ice-cold lysis buffer (PBS + 0.1% IGEPAL CA-630 (Sigma, Cat# I3021) containing freshly added protease inhibitor cocktail (Roche, Cat# 04693116001) and centrifuged at 13,000 g for 10 min at 4°C. Total protein concentration of the supernatant was measured using the BCA assay (Pierce BCA Protein Assay Kit, Thermo Fisher Scientific; Cat# 23227). CSF was extracted through a glass pipette using a refined cisterna magna puncture technique ([Liu and Duff, 2008](#)). CCL2 concentration was measured using mouse (R&D Systems, Cat # MJE00) or human (R&D Systems, Cat# DCP00) ELISA kit. Protein level of various cytokines in the mouse hippocampus was measured with mouse cytokine/chemokine magnetic bead panel 96-well plate assay (R&D Systems, Cat# MCYTOMAG-70K). Data were collected on a Luminex200/MAGPIX system at the Merck Biomarker Service Lab in Shanghai and analyzed using MILLIPLEX Analyst.V5.1 (Millipore).

Ccr2 RNAi Virus and In Vivo Stereotaxic Viral Injections

Mouse Ccr2 shRNA sequence (TGCTAACGTCTGCAA) ([Leuschner et al., 2011](#)) was subcloned into the pFUGW-RNAi lentiviral vector by Genechem (Shanghai, China); shRNA was expressed under the U6 promoter and GFP was expressed under the ubiquitin promoter. P8 mice were anaesthetized with 0.04 g/kg sodium pentobarbital, 0.6 µL lentiviruses (6×10^8 transducing units (TU)/µl, packaged by Genechem, Shanghai, China) were slowly injected into the left hippocampus at a speed of 60 nl/min, as previously described ([Zheng et al., 2014](#)). Experiments were carried out 5 days or longer after viral injection, to allow time for gene expression.

Cell Culture and Transfection

Neuro2A cells were cultured using standard protocol described by ATCC and in DMEM/F12 medium (Thermo Fisher Scientific, Cat# 11320033), supplemented with 10% Fetal Bovine Serum (Thermo Fisher Scientific, Cat# C838T52). Neuro2A cells are male cells. Full-length of Ccr2 cDNA was subcloned from mouse tissue and fused with in frame with GFP. Transfection of Neuro2A was performed with pCAGGS-CCR2-GFP and CCR2-RNAi ([Leuschner et al., 2011](#)) plasmids using Lipofectamine 2000 (Thermo Fisher Scientific, cat# 11668019) according to the manufacturer's protocol. The cells were harvested 48 h after transfection and analyzed by immunoblot using antibody against GFP (1:1000, Invitrogen, Cat# A11122) and GAPDH (1:5000, KangChen Biotech, Shanghai, China, Cat# KC-5G4).

Western Blots

Mice were deeply anaesthetized using 0.14 g/kg sodium pentobarbital. Hippocampi were quickly dissected, and membrane fractions were collected. Western blots and sample preparation were performed as previously described ([Zheng et al., 2014](#)). Blots were visualized using ECL chemiluminescence substrate (Thermo Fisher Scientific) and X-ray films (Kodak, Rochester, NY, USA) or Amersham Imager 600 (GE Healthcare, Chicago, IL, USA). Blots were quantitated using Fiji/ImageJ. GluA1 (1:1000, Millipore, Cat# AB1504) and GAPDH (1:5000, KangChen Biotech, Cat# KC-5G4) antibodies were used.

Acute Brain Slice Preparation

Mice were deeply anesthetized with 0.7% sodium pentobarbital at 0.14 g/kg body weight, and acute brain slices were prepared as described previously ([van Praag et al., 2002](#)). For P14 mice, brains were rapidly removed and immersed in ice-cold choline based dissection buffer containing the following (in mM): 110 choline-Cl, 2.5 KCl, 1.3 NaH₂PO₄, 7 MgCl₂, 0.5 CaCl₂, 25 NaHCO₃, 15 D-glucose, bubbled with 95% O₂/5% CO₂, pH 7.4. For adult mice, mice were perfused with N-Methyl- D -glucamine (NMDG) based dissection buffer, and brains were removed and immersed in ice-cold based dissection buffer containing the following (in mM): 93 NMDG, 2.5 KCl, 1.2 NaH₂PO₄, 10 MgSO₄, 0.5 CaCl₂, 20 HEPES, 3 sodium pyruvate, 30 NaHCO₃, 25 D-glucose (adjust to pH7.4 with 10N HCl), bubbled with 95% O₂/5% CO₂. Hippocampal and cortical slices were cut at 250 µm thick using a vibratome slicer (VT 1200s, Leica Microsystems, Nussloch, Germany) in dissection buffer. For P14 mice, slices were allowed to

recover in a submersion holding chamber with artificial CSF (aCSF) containing (in mM): 125 NaCl, 2.5 KCl, 1.3 NaH₂PO₄, 1.3 MgCl₂, 2 CaCl₂, 25 NaHCO₃, 15 D-glucose, bubbled with 95% O₂/5% CO₂ for 30 min at 37°C, followed by least 1 h recovery at 26°C before recordings. For adult mice, slices were allowed to recover in a submersion holding chamber with NMDG based dissection buffer bubbled with 95% O₂/5% CO₂ for 7 min at 32°C, followed by least 1 h recovery at 26°C before recordings.

Whole-Cell Recordings

For recordings, individual slices were transferred to a submersion recording chamber and were continuously perfused with 95% O₂/5% CO₂ bubbled with aCSF at 28–30°C. Slices were visualized with an upright microscope (BX51WI, Olympus, Tokyo, Japan) equipped with differential interference contrast optics and an infrared CCD camera (IR-1000E, DAGE-MTI, Michigan, IN, USA). Recordings were made from neurons in hippocampal CA1, CA3, dentate gyrus, or cortical primary somatosensory areas (S1), with a MultiClamp 700B amplifier (Molecular Devices, Sunnyvale, CA, USA). Signals were low-pass filtered at 2 kHz and sampled at 10 kHz using Digidata 1440A (Molecular Devices).

For mEPSC recordings, glass pipettes (resistance, 3–5 MΩ) were loaded with internal solution containing (in mM): 100 CsMeSO₄, 25.5 CsCl, 10 HEPES, 8 NaCl, 0.25 EGTA, 10 D-glucose, 2 MgATP and 0.3 Na₃GTP (pH 7.3, 290 mOsm), and all neurons were held at -70 mV in voltage-clamp mode; 10 μM gabazine and 1 μM TTX were added to aCSF to block GABA_A and Na⁺ currents, respectively. BAPTA tetracesium (5 mM) was added to the internal solution to block Ca²⁺-induced effects.

For mIPSC recordings, a high chloride internal solution containing (in mM): 110 CsCl, 10 NaCl, 5 MgCl₂, 0.6 EGTA, 2 MgATP, 0.2 Na₃GTP and 40 HEPES (pH 7.3, 290 mOsm) was used, and cells were held at -60 mV in voltage-clamp mode; 10 μM NBQX and 1 μM TTX were added to block AMPA and Na⁺ currents, respectively.

For all mPSC recordings, a brief hyper-polarization step (-10 mV, 100 ms) was given to monitor series and input resistances every 10 s. Cells were excluded from analysis if their input resistance fluctuated by more than 20% or if series resistance exceeded 30 MΩ. Series resistances were not significantly different between experimental groups. Liquid junction potential and series resistance were uncompensated.

The spike frequency versus injected current experiments were performed by measuring the average action potential firing rate during 500 ms depolarizing current injections of 20 pA increments (10 pA for dentate gyrus), in current-clamp mode. The maximum current injected in each experiment was below the current that induced adaptation. The first step current which induced a spike was defined as the rheobase current. Synaptic blockers (50 μM D-APV, 10 μM NBQX, and 10 μM gabazine) were included as indicated. The internal solution contained (in mM): 110 K-gluconate, 20 KCl, 20 HEPES, 5 MgCl₂, 0.6 EGTA, 2 MgATP, 0.2 Na₃GTP (pH 7.3, 290 mOsm).

Evoked EPSC, AMPA/NMDA ratio and paired-pulse ratio were recorded in aCSF containing 10 μM gabazine. A glass pipette filled with aCSF was placed in the stratum radiatum, and generated a brief stimulation pulse (1 ms) under the control of Digidata 1440A (Molecular Devices) and Iso-Flex isolator (A.M.P.I., Jerusalem, Israel). Minimal evoked EPSC was recorded at a stimulation strength which induced both EPSCs and failures, with a failure rate of approximately 50%. AMPA receptor and NMDA receptor-mediated EPSCs of hippocampal CA1 pyramidal neurons were recorded at holding potentials of -70 mV and +40 mV, respectively. AMPA receptor-dependent EPSCs were quantified by measuring the peak amplitude after the onset of synaptic responses, while NMDA receptor-dependent EPSC amplitudes were measured 50 ms after EPSC onset, as previously described (Peng et al., 2010). Paired-pulse ratio (PPR) was measured as the ratio of the second EPSC to the first one.

In CCL2 application experiment, CCL2 was perfused onto slices at 100 ng/ml, based on previous investigations in other systems (Gao et al., 2009; Gosselin et al., 2005). In CCL2 mPSC experiments, baseline (Ctrl) recordings were from 0 – 5 min before CCL2 application, while CCL2 recordings were from 5 – 10 min after CCL2 perfusion. For all other experiments, recordings from Ctrl and experimental conditions were interleaved. To investigate the effect of stimulated HBVP ECS, brain slices were incubated with HBVP-conditioned Ctrl ECS, LPS/Poly(I:C) stimulated ECS or antibody neutralized ECS for 30 min at 26°C before recordings. LPS/Poly(I:C) were washed out from the stimulated ECS (see ECS collection section for details).

All salts and drugs were obtained from Sigma or Tocris Bioscience, except for TTX, which was obtained from the Fisheries Science and Technology Development Company of Hebei Province, China.

Data were analyzed in Clampfit 9 (Molecular Devices), except for the amplitude and frequency of mPSCs, which were analyzed in MiniAnalysis (Synaptosoft, Fort Lee, NJ, USA) with detection thresholds of 5 pA. The total charge per second was calculated by summing the area of each mPSC event, per unit time. Data analysis was carried out blinded to the experimental condition.

Single-Cell RNA Sequencing and Data Processing

Three independent sets of experiments were carried out. In each experiment, P14 mice were i.p. injected with saline (control) or 10 mg/kg LPS, and sacrificed 2 hr later. Acute brain slices were prepared as for electrophysiological experiments (see above for details). Each sample contained brain slices from one male and one female mouse, to reduce batch effects. After the brain slices recovered, hippocampi were dissected and dissociated using the Papain Dissociation System (Worthington, Lakewood, NJ, USA; Cat# LK003153) according to the manufacturer's instructions. The cell suspension was filtered with a 40 μm filter (Thermo Fisher Scientific, Cat# 352340) and resuspended in DMEM (Thermo Fisher Scientific, Cat# 12800017) containing 10% Fetal Bovine Serum (Thermo Fisher Scientific, Cat# C838T52). Single cells were captured using the 10X Chromium (10X Genomics, Pleasanton, CA, USA), and

libraries were prepared according the manufacturer's instructions (Chromium Single Cell 3' Library & Gel Bead Kit v2, 10x Genomics). Sequencing was performed on the Illumina NovaSeq 6000 (by Novogene, Beijing, China).

Sequencing data were processed with the 10X Cell Ranger (10X Genomics), to normalize the sequencing depth of different conditions and batch (using the "cellranger aggr" function). The post-normalization mean reads per cell is 146,673; the median genes per cell is 2957. The normalized data were further analyzed using Seurat v2.2. Genes and cells were selected according to the following criteria: 1) genes were expressed by at least 3 cells; 2) cells that expressed 600 and less than 7500 genes; 3) the percentage of mitochondrial genes per cell was less than 25%. 9957 cells in the control group and 9675 cells in the LPS group fulfilled these criteria and were further analyzed. We used "LogNormalize" (scale factor: 10,000) to normalize gene expression in each cell. The influence of batch effects and percentage of mitochondrial genes in each group/condition were regressed out using Seurat v2.2. The top 1000 variable genes of each group were selected for canonical correlation analysis using the RunCCA function (num.cc = 35). According to the MetageneBicorPlot and the DimHeatmap, we chose the first 30 CCs to align the CCA subspace. RunTSNE and FindClusters functions were used for visualization (dim.use = 1:30) and clustering (dim.use = 1:30, resolution = 0.3). At resolution of 0.3, 19 clusters were identified, including distinct clusters for *Col1a1* and *Rgs5* cells. At the lower resolution of 0.1, 15 clusters were observed and the above mentioned clusters were merged. We used the higher resolution in our analyses, because *Col1a1* cells are more responsive to LPS treatment than *Rgs5* cells, and these cells have other characteristics that are distinct from each other. Thus we believe that it would be important to describe them separately. We did not use even higher resolution because it would also separate other clusters into more sub-clusters, making the data more complicated to read.

The cell markers of different clusters were identified using the FindConservedMarkers function. The LPS responsive genes in each cell cluster were identified using the FindMarkers function.

Immunocytochemistry

Cultured HBVP were washed in phosphate-buffered saline (PBS) and fixed in 4% paraformaldehyde (Sigma, 441244) in PBS for 20 min at room temperature. They were then permeabilized for 5 min with 0.1% Triton X-100 in PBS, and blocked with 3% bovine serum albumin (BSA, Calbiochem) in PBS for 1 h at 37°C. Primary and secondary antibody incubations (both in 3% BSA) were overnight at 4°C and 2 h at 37°C, respectively. Primary antibodies used: Anti-MCP1 antibody (Abcam, Cat# ab9669, 1:200), NFκB p65 (C20; Santa Cruz, Cat# SC-372, 1:100), PDGF R beta antibody (R&D, Cat# AF1042, 1:200). The following secondary antibodies (all from Thermo Fisher Scientific): Donkey anti-Rabbit Alexa Fluor 488 (Cat# A21206), Donkey anti-Rabbit Alexa Fluor 568 (Cat# A10042), Donkey anti-Goat Alexa Fluor 488 (Cat# A11055), Donkey anti-Goat Alexa Fluor 568 (Cat# A11057) were used at 1:1000, and DAPI (Thermo Fisher Scientific, Cat# D1306) was used at 1:3000. Coverslips were mounted in Fluoromount Aqueous Mounting Medium (Sigma, Cat# F4680).

Fluorescent *In Situ* Hybridization, RNAscope, and Immunohistochemistry

Mice were deeply anaesthetized with 0.14 g/kg sodium pentobarbital and perfused with diethylpyrocarbonate (DEPC)-treated phosphate-buffered saline (PBS, pH 7.4, 37°C), followed by cold 4% diethylpyrocarbonate (DEPC)-treated paraformaldehyde (PFA, w/v) in PBS. Brains were carefully dissected out using surgical scissors. For immunohistochemistry and RNAscope, brains were post-fixed in 4% PFA at 4°C for 24 h, cryoprotected in 30% sucrose (w/v) in PBS for at least 2 days at 4°C, and sectioned using a cryostat (CM1950, Leica Microsystems). For *in situ* hybridization, brains were post-fixed in 4% PFA overnight at 4°C, and sectioned using a vibratome (VT1000S, Leica Microsystems). *In situ* hybridization was performed according to previously published protocols (Wu et al., 2009; Xiu et al., 2014). For *in situ* hybridization and RNAscope, all solutions were prepared using diethylpyrocarbonate (DEPC)-treated double deionized water (ddH₂O) and RNase-free reagents, and all instruments were RNase-decontaminated using Ambion RNase Away Decontamination Reagent (Ambion, Cat# 10328011).

For *in situ* hybridization, probes were generated using the following primers and cloned into pBluescript:

Ccl2_Probe_1-Forward primer: CCAGCACCGCCAACCTCT
Ccl2_Probe_1-Reverse primer: GGTGTACAAAAATAATATAT
Ccl2_Probe_2-Forward primer: TCTCACTGAAGCCAGCTCT
Ccl2_Probe_2-Reverse primer: CATCACAGTCCGAGTCACAC (Miller et al., 2012)
Vtn_Probe_1-Forward primer: TGCGACTACATGGAGCA
Vtn_Probe_1-Reverse primer: GCCATAGCAGCGTCCACT (Allen Brain Atlas; probe: RP_040922_01_C11)

RNA probes were labeled using either the DIG RNA Labeling Mix (Roche, Cat# 11277073910) or the Fluorescein RNA Labeling Mix (Roche, Cat# 11685619910) and generated by *in vitro* transcription. Coronal, free-floating sections (40 μm) were sequentially treated with 2% H₂O₂ (vol/vol) in PBS for 10 min, 0.5% Triton X-100 (vol/vol) in 2x SSC for 30 min, and 0.25% acetic anhydride (vol/vol) in 0.1 M triethanolamine (pH 7.5) for 10 min, with extensive washes in PBS between procedures. Sections were then incubated in the prehybridization solution [50% formamide (vol/vol), 5 × SSC, 0.1% Tween 20 (vol/vol), 0.1% 3-[(3-cholamidopropyl) dimethylammonio]-1-propanesulfonate (CHAPS, wt/vol) and 5 mM EDTA] for 2 h at 65°C, before probes were added at 0.5 μg/ml. Probes were dissolved in hybridization solution [50% formamide (vol/vol), 5 × SSC, 0.3 mg/ml yeast tRNA, 100 μg/ml heparin, 1 × Denhardt's

solution, 0.1% Tween 20 (vol/vol), 0.1% 3-[(3-cholamidopropyl) dimethylammonio]-1-propanesulfonate (CHAPS, wt/vol) and 5 mM EDTA]. Sections were incubated with probes for 16–18 h at 55°C, washed in prehybridization solution for 30 min at 65°C, in TBST and prehybridization mix solution (vol/vol = 1:1) for 30 min at 65°C, in TBST for 5 min twice at room temperature, rinsed with TBST and TAE mix solution (vol/vol = 1:1), washed in TAE for 5 min 3 times, and subjected to electrophoresis (60 V, 2 h) to remove unhybridized probes (Kobayashi et al., 1994). Sections were then incubated for 12–18 h at 4°C in buffer containing primary antibody. For DIG labeling, anti-Digoxigenin-AP Fab fragments (Roche, Cat# 11093274910, 1:2000) or anti-Digoxigenin-POD Fab fragments (Roche, Cat# 11207733910, 1:4000) were used. For fluorescein labeling, peroxidase-IgG fraction monoclonal mouse anti-fluorescein (Jackson ImmunoResearch, Cat# 200-032-037, 1:4000) was used. For examining colocalization with various cell type markers, fast red (Roche, Cat# 11496549001 or Sigma, Cat# F4523) or the tyramide signal amplification (TSA) plus cyanine 3 system (PerkinElmer, Cat# NEL744) was used for visualization. For colocalization experiments using transgenic mice, TSA plus DNP system (PerkinElmer, Cat# NEL747A), together with anti-DNP-488 (Invitrogen, Cat# A-11097, 1:1000) or the TSA-plus Cyanine 5 system (PerkinElmer, Cat# NEL745) was used, according to the manufacturer's instructions.

For RNAscope, 20 µm coronal sections were mounted onto SuperFrost Plus Slides (Fisher Scientific; Cat# 12-550-15) and air-dried. Sections were processed using RNAscope Multiplex Fluorescent Reagent Kit v2 (Advanced Cell Diagnostics, Newark, CA, USA; Cat# 323100), according to the manufacturer's instructions. Probes against *Ccl2* (Advanced Cell Diagnostics; Cat# 311791) and *Col1a1* (Advanced Cell Diagnostics; Cat# 319371) mRNA were used.

When immunohistochemistry was carried out together with fluorescent *in situ* hybridization (FISH), the following primary antibodies used include: mouse PDGF R beta (R&D, Cat# AF1042, 1:100), glucose transporter GLUT-1 (Millipore, Cat# CBL242, 1:100), glial fibrillary acidic protein (GFAP; Dako, Cat# Z0334, 1:500), Iba1 (Wako, Cat# 019-19741, 1:500) and tdTomato (SICGEN, Cat# AB8181-200, 1:500). Secondary antibodies are same as for immunocytochemistry. Sections were incubated with DAPI for 30 min at room temperature prior to mounting onto glass slides.

Image Acquisition and Image Analysis

Whole brain images were acquired on an Olympus VS120 confocal microscope with UPLSAPO 20x objective (N.A. = 0.75) or a Nikon A1 plus confocal microscope with Plan Apo λ 10x (N.A. = 0.45). Astrocytes and microglia activation images were acquired on Nikon A1 plus with Plan Apo λ 20x (N.A. = 0.75). All other images were acquired on a Nikon A1 Plus with Apo 60x Oil λS DIC N2 objective (N.A. = 1.40) or an Olympus FV10I confocal microscope with an Apo 60x Oil objective (N.A. = 1.35).

Image analysis was performed using Image-Pro Plus (Media Cybernetics, Rockville, MD, USA) and/or ImageJ/Fiji (N.I.H., Bethesda, MD), blinded to the experimental condition. For colocalization experiments, images for each channel were separately thresholded, and colocalization was defined as at least one pixel of overlap between the two channels. For colocalization of *Ccl2* with various markers, the area of *Ccl2* colocalizing with each marker was ratioed over that of total *Ccl2* area. For measuring the percentage of nuclear NFκB in HBVP, colocalization was defined as at least one pixel of overlap between NFκB immunostaining and DAPI. For measuring the level of Iba1, GFAP and *CCL2*, total intensity and/or area was ratioed over that of DAPI area.

Images analysis was carried out with no post-acquisition modifications. For example images, brightness/contrast were adjusted within linear ranges using Fiji/ImageJ when necessary. Control and experimental conditions were adjusted with the same parameters.

Tail Suspension Test

Mice were suspended by the tail, with the distance between the mouse's nose and the apparatus floor being 20 cm. Mice were positioned such that their ventral side faced the camera. Behavior was analyzed for a 6 min time window, beginning with the suspension of the mouse. Immobility time was defined as time during which the percentage change in object area between video frames was below a defined mobility threshold (Juszczak et al., 2006). Data analysis was automated and blinded to the experimental condition.

Blood-Brain Barrier Permeability Test

Adult mice were injected from the caudal vein with 2 mL/kg Evans blue dye (2% in saline). One hour after injection, mice were anesthetized and perfused with saline, followed with 4% paraformaldehyde (PFA). Brains were then post-fixed in 4% PFA for 6 h and dehydrated with 30% sucrose for 3 days. They were then coronally sectioned into 40 µm slices. Brain slices were incubated with DAPI for 30 min at room temperature prior to mounting on glass slides. Evans blue total intensity was ratioed over that of DAPI area.

QUANTIFICATION AND STATISTICAL ANALYSIS

Statistical analysis was performed using GraphPad Prism 7 (GraphPad Software, La Jolla, CA, USA). No statistical methods were used to predetermine sample sizes; however, our sample sizes are similar to those reported in previous publications (Norden et al., 2016; Zheng et al., 2014). No randomization algorithm was used, although mice were randomly assigned to experimental conditions. Data were analyzed blinded to the experimental condition. Data are presented as mean ± SEM. Gaussian distribution of the data was assessed using Shapiro-Wilk normality test, KS normality test or D'Agostino & Pearson normality test. If the data pass the

Gaussian distribution test, parametric tests (paired or unpaired t test for two groups) were used, otherwise nonparametric tests (Wilcoxon matched-pairs signed rank test for paired groups, Mann-Whitney for unpaired two groups, and Kruskal-Wallis test, followed by Dunn's multiple comparison test for three or more groups) were used. For excitability experiments, two-way ANOVA followed by Bonferroni's multiple comparisons test was used.

DATA AND SOFTWARE AVAILABILITY

The accession number for the single cell RNA-seq data in GEO is GSE112436.